CLM-R.107

CLM-R 107

United Kingdom Atomic Energy Authority
RESEARCH GROUP
Report

MEASUREMENT OF THE PLASMA PARAMETERS IN TOKAMAK T3-A BY THOMSON SCATTERING

M. J. FORREST
N. J. PEACOCK
D. C. ROBINSON
V. V. SANNIKOV
P. D. WILCOCK

Culham Laboratory
Abingdon Berkshire
1970
Available from H. M. Stationery Office
SEVEN SHILLINGS NET
C.18

U.D.C.
533.9.082.5 : 621.375.826
621.039.626 TOKAMAK
621.039.66

MEASUREMENT OF THE PLASMA PARAMETERS IN TOKAMAK T3-A BY THOMSON SCATTERING

by

M.J. Forrest, N.J. Peacock, D.C. Robinson, V.V. Sannikov*
P.D. Wilcock

A B S T R A C T

The electron temperature and density in Tokamak T3-A are established from an analysis of the spectral intensity of the scattered photons from a pulsed ruby laser. Electron temperatures up to 2 keV are measured over a range of densities from 1 to $4{\cdot}5 \times 10^{13}$ cm^{-3} and ohmic heating currents up to 150 kA. Radial measurements show the pressure profile to be practically flat over the central half of the plasma. The total energy in the plasma column agrees with that measured from the diamagnetic signal. The dependence of the temperature on the discharge parameters is expressed by the relation, $I^2\beta_\theta = 200\ Nk(T_e + T_i)$, where β_θ with respect to the heating current is 0·5 in the middle of the current pulse. The value of β_θ reaches 2, which is close to the limit set by classical diffusion, when dI/dt is negative, late in the current pulse. The local temperature rise in the outer region of the discharge due to skin currents, is weak, and after the initial increase of the current, is negligible. The resistivity is always anomalous except late in the current pulse and is associated with a critical value for the ratio of the drift to sound speed. The measured particle loss time (which has almost the classical value) is always 3 or 4 times the energy loss time. It is shown by considering the energy balance, taking into account the anomalous factor in the heating, that the main energy loss is by heat conduction which is anomalously large for all but the highest densities.

*Kurchatov Institute, Moscow

U.K.A.E.A. Research Group,
Culham Laboratory
Abingdon
Berks

July, 1970

CONTENTS

1. INTRODUCTION

Much of the widespread interest in the Tokamak devices arises from the high total energy in the plasma column[10] and the long energy containment time[3]. Conclusions on these aspects of Tokamak have been based largely on measurements of the plasma energy using the diamagnetic technique[19]. Interpretation of the diamagnetic signal per se is ambiguous to the extent that a distorted Maxwellian distribution with a relatively small number of high energy electrons could account for the total electron energy as readily as a thermal distribution.

The photon scattering technique offers a direct and independent measurement of both the electron energy distribution and the electron density locally in the plasma.

A preliminary account of these scattering experiments has already been published[22]. The present report describes the experiments more fully and includes the analyses of scattering measurements over a wider range of discharge parameters. From the absolute intensity of Balmer α emission the particle confinement time is also evaluated. A documentation of the light-scattering results is provided in Sections 7 to 11 while a summary of these results is given in Section 14. In the work presented emphasis is given to the scattering results and these are sufficiently informative to allow conclusions to be made on the physical properties operative in T3, and these are discussed in Sections 15 to 20.

Reference is made to the results of the analysis of the electrical waveforms in order to support the discussion Section. However, a more detailed discussion of the electrical measurements and a comparison of the scattering results with the diamagnetic energy has been submitted for publication elsewhere[11,12].

2. TOKAMAK T3-A

The Tokamak T3-A torus used in the scattering measurements has a major radius, R, of 1 metre. A 20 cm radius, stainless steel liner, which encloses the discharge volume is shrouded by an outer copper shell, 25 cm in radius and 3 cm thick. The volume between the liner and the copper shell is evacuated and the background pressure within the inner torus is less than 10^{-7} Torr. A molybdenum limiter, 17.5 cm radius, physically restricts the discharge.

The main toroidal field, B_o, with values up to 37 kilo-oersted, is produced from rotating machinery in a 1 s pulse. The ohmic heating current, I, is supplied from 3 capacitor banks which are switched separately (with a current rise-time of 4 ms) to provide a current pulse which is variable up to 180 kA peak value, and with a pulse duration up to 70 ms. The vertical field, which controls the plasma displacement, has a DC component on which is superimposed a pulsed component supplied from windings inside the copper shell.

The operating conditions were generally chosen so that the plasma was located in the stable regime with the stability factor, $q = \frac{B_o}{B_\theta}\frac{r}{R} > 3$, although some marginally stable plasmas were also studied with q between 2 and 3 (B_θ is the poloidal field due to the current, I, while r is the plasma radius).

In order to achieve a clean, reproducible plasma it was the practice to bake out the inner chamber under vacuum for several days at over 400°C and then fire several hundred 'conditioning' discharges at very low pressure.

The gas filling for each plasma shot was admitted at a pressure of between 1 and 10×10^{-4} Torr, through a pulsed valve and the plasma formation assisted using a hot filament.

3. EXPERIMENTAL ARRANGEMENT

Because of the geometrical disposition of the existing windows in the T3-A diagnostic flange, it is most convenient to project the laser beam vertically upwards through the minor cross-section of the torus, parallel to the major axis, while the scattered light is observed at 90^{o} to the irradiating beam as shown in Fig.1. A ruby laser is chosen because of its inherent brightness in the visible where the quantum efficiency of the detector is high.

In the case that the differential scattering vector $K = \frac{4 \pi \, \mathrm{Sin}\, \theta/2}{\lambda_o}$ is greater than λ_D^{-1}, (λ_D is the debye length in the plasma, θ is the angle between the incident and scattered beams and λ_o is the laser wavelength), the frequency shifts of the scattered photons are directly due to the uncorrelated motions of the electrons. These conditions obtain in T3-A with the above geometrical arrangement and where the density from 2 mm μwave measurements[9] is about 10^{13} cm^{-3} and where the temperature (deduced from the soft X-ray spectrum in TM3[27]), is expected to be in the region of 1 keV.

The scattering parameter $\alpha = \frac{1}{K\lambda_D} \lesssim 0.1$, and no co-operative features are to be expected. With a Maxwellian velocity distribution the scattered spectrum has then a gaussian profile

$$I_s = C. \frac{\lambda_o}{\mathrm{Sin}\, \theta/2 \sqrt{T_e}} \exp - \left\{ \frac{2.63 \times 10^{-3} \Delta\lambda^2}{T_e} \right\} \qquad \Delta\lambda \text{ in Å}, \; T_e \text{ in eV} \qquad \ldots (1)$$

and the total intensity of the scattered light is linearly proportional to the electron density. Scattering from plasma particles other than electrons (e.g. excited atoms[25]) can be ignored since the excited states of impurity ions in the plasma with quantum jumps close to the laser energy should be negligibly populated, at kilovolt temperatures.

The spectrum analyser, a ten-channel, 1 metre, Ebert spectrometer is optically matched to the light collecting lens by opening up the spectrometer entrance slit to 1 cm. The effective aperture of the system was F/6. The resulting width of monochromatic light on the focal plane of the spectrometer with a 1200 lines/mm grating is thus (78 Å/mm) x 10 mm = 78 Å, and this is the wavelength range (and therefore the resolution) accepted by each fibre optic bundle which leads the light signals to the ten, S20 photocathode, photomultipliers. Since the $\frac{1}{e}$ intensity points of the scattered photon intensity lie at

$$\Delta\lambda_{\frac{1}{e}} = 19.3 \sqrt{T_e} \text{ Å}; \quad T_e \text{ in eV} \qquad \ldots (2)$$

from the laser wavelength; temperatures in the range 50 to 2000 eV can be resolved. The outputs from photomultipliers through X 15 current gain amplifiers (Fig.2) are led to separate beams of high speed oscilloscopes. Because of the limited quantum efficiency of the S 20 photocathode in the infra-red all the measurements of the spectrum profile are taken at wavelengths shorter than the ruby wavelength of 6943 Å.

The collecting lens (Fig.1) views an elliptically shaped (7 x 3 x 5 mm), 0.1 cm^3 volume irradiated by the laser but at the same time accepts background light from 10 cm^3 of the

plasma. The wedged collection lenses and the moveable periscope allow a radial scan of the plasma to be made from - 10 cm to + 18 cm about the magnetic axis. Except when in use the windows are protected from metallisation due to pre-conditioning discharges by shutters (see Fig.1) which can be actuated through tombac vacuum seals.

4. NOISE PROBLEMS

Each 78 Å wide channel carries only about 10^{-16} of the irradiating photon flux so it is important to suppress spurious sources of noise such as the inherent (wide-band) radiation from the plasma and the parasitic (narrow-band) scatter of the 6943 Å beam by the input and dump optics.

In practice, the brightness (watts/sterad. $cm^2 \cdot$ sec) of the input beam has to be sufficiently high for the scattered photon flux to be of the same order as the plasma background illumination. Thus the Thomson scattering/Bremsstrahling ratio can be expressed as

$$\frac{I_o \, \sigma_T \, n_e \, \frac{\delta\Omega}{4\pi} \, \delta\lambda \, S(\Delta\lambda) \, Vs}{2 \times 10^{-36} \, \frac{n_e^2}{\lambda^2} \, \frac{\delta\lambda}{\sqrt{W}} \, \frac{(\delta\Omega)}{4\pi} \, Vp} \quad \ldots (3)$$

where I_o is the incident laser power, $S(\Delta\lambda)$ is the wavelength spectrum of the scattered light which when integrated over $\Delta\lambda$ is unity. The Thomson scattering cross section $\sigma_T = 6.65 \times 10^{-25}$ cm^{-3}, $\frac{\delta\Omega}{4\pi} = 1.8 \times 10^{-3}$ steradians, $\delta\lambda = 78$ Å, V_s, the irradiated volume = 0.1 cm^3, and V_p, the plasma volume accepted by the collecting lens, 10 cm^3. In a pure hydrogen plasma at a density of 10^{13} cm^{-3} and a temperature of 1 keV, the scattered photon flux per channel from a laser giving 100 joules in 1 ms (a typical relaxation mode pulse) approximates to the light collected from the plasma itself, $\sim 10^4$ photons, these photons being integrated over the 1 ms pulse (the transmission of the spectrometer is approx. 10%). Fig.3 shows the results of an attempt to record scattering on this basis. The intense radiation at the beginning of the pulse decreased to a low value after 8 ms (normally the experimental procedure to protect the photomultipliers from this initial intense light involves opening a mechanical shutter in front of the spectrograph 1 ms before the laser is fired). The only signal observed at about 16 ms, in Fig.3, is on the channel centred on 6943 Å and is due to parasitic scatter.

Measurement of the absolute intensity of the background radiation (Fig.4) shows this to exceed by a factor of 200, the anticipated level from a hydrogen plasma - thus the use of a relaxation mode pulse was not possible. The intense peak at 6593 Å (Fig.4) due to Balmer α, is smeared over two channels and is thus twice the width of a monochromatic line. The background light was found to be line emission which originates from a region outside the radius of the limiter which is located at 17·5 cm from the centre of a minor cross section. These lines are mainly due to spark spectra of iron, typical examples of which in the region 6500 Å - 6300 Å, are the Fe I, II lines at 6498, 6446, 6400, 6408, 6412, 6419, 6337, 6335 and 6332 Å. The intensity of this background line radiation increases as the square of the electron density, (Fig.5), so that no improvement in signal ($\propto n_e$) to noise ($\propto \sqrt{n_e^2}$) is to be expected by varying the density.

To overcome the background illumination the ruby laser is employed in the Q-switched mode using an oscillator and X 15 gain amplifier. The output used in all these experiments

is 6 joules in 25 ns with a beam divergence of 2.5 mrad. This resulted in an improvement in signal to noise over the relaxation mode pulse by a factor of 2×10^3, and Thomson scattered signals at 10 times the noise level were readily obtained.

The Q-switched mode has the limitation that at low densities the absolute number of photoelectrons per signal channel is low (of the order 10 to 100 in our experiments at $n_e \simeq 10^{13}$ cm^{-3}) because the energy density in the input beam has to be kept below 1 GW cm^{-2} to prevent damage to the input window. In practice this is effected by opening the oscillator aperture from ¼" to ⅜" and adjusting the pumping energy thus increasing the divergence of the laser beam.

It is clear that with the present apparatus, on T3-A, the lower density limit for recording meaningful scattering signals is about 8×10^{12} cm^{-3}. With readily available improvements e.g. higher quantum efficiency photomultipliers, measurements at densities of $\sim 2 \times 10^{12}$ cm^{-3} could be made using the Q-spoiled technique. Parasitic scatter is always observed on the channel centred on 6943 Å with an intensity about 200 times the genuine scattered signal. Rayleigh scattering from clean nitrogen in the Tokamak chamber established that the parasitic noise is equivalent to the scatter from cold electrons at a density of 1 to 2×10^{14} cm^{-3}. The contrast of the spectrometer is sufficiently high (~1500) to ensure that the other channels are free of this source of noise, however a slight deterioration in the surface finish of the plane, input spectrosil window caused the parasitic noise to increase and spill over into these adjacent channels. A major factor in keeping the parasitic noise low is the disposition of absorbing, dyed-glass (OB10) apertures (Fig.1) both inside and outside the input window.

5. THOMSON SCATTERED SIGNALS

The shape of the scattered light pulse is shown in Fig.6 while the relative magnitudes of two channels, displaced 156 Å, 234 Åand 546 Å respectively from the laser wavelength, are illustrated on Fig.7. A considerably smaller ratio of signal to noise than is evident in Fig.7 is experienced when the laser is fired early ($\lesssim$ 4 ms) in the discharge pulse or when the irradiated plasma is viewed at radii > 12 cm from the magnetic axis, since under these conditions the background light from the plasma is relatively high. Furthermore the density in the outer region is appreciably less than at the centre.

Two tests were carried out which demonstrated that the plasma electrons are responsible for the scattered light signals shown in Fig.7. Firstly, when the collecting lens (Fig.1) viewed a plasma volume adjacent to the irradiated plasma, no signals were observed. Secondly, changes in the plasma density (measured on the multi channel μ-wave interferometer) cause a linearly proportional variation in the total scattered light intensity.

6. SPECTRAL DISTRIBUTION AND INTENSITY OF THE SCATTERED LASER LIGHT

Taking into account the measured relative sensitivity of each 78 Å wide channel, the spectrum of the scattered light, for wavelengths shorter than the ruby light, could be plotted out as a function of the square of the wavelength shift; Fig.8. The straight line plot is characertistic of a thermal spread in velocities associated with an electron temperature of 640 eV. Fig.9 shows the measured spectral distribution and theoretical gaussian profiles for three different plasma conditions. The temperatures vary in this illustration from 100 eV to 1 keV. The errors on the experimental points are typically the standard

deviation of the signals over 5 to 10 discharges under the same operating conditions. Errors in estimating the temperature (Fig.8) from a best fit straight line through the experimental points are between 5 and 15% for most of our results. For the limits of our temperature range, i.e. < 100 eV or > 1.5 keV, the errors could be as high as 20%. Departures from a gaussian distribution due to current drift are only of the order of a few per cent, and in any case are not detectable using our scattering geometry. Again our errors could obscure the small distortion to the gaussian at some radial distance from the axis due to trapped particle orbits.

Some variation in the value of the temperature for nominally the same discharge conditions may be noted in the figures of the results. This variation is sometimes outside the errors quoted above and can be attributed to irreproducibility of the discharge and to errors in the timing of the laser pulse relative to current zero.

The response of each of the recording photomultiplier channels and the transmission of the spectrograph was measured absolutely during each experimental run using a tungsten ribbon lamp of known spectral emission as a source of photons which substitutes for the irradiated plasma volume. The entrance slit of the spectrometer was illuminated via an identical set of optics as that used for collecting the scattered photons but with a mirror in front of the periscope, set at 45^{o} to the spectrometer optic axis (Fig.1). The continuous flux from the lamp is modulated by a 1 kHz mechanical chopper in front of the spectrometer slit.

Account is taken of the change in frequency response from the Q-spoiled pulse to the 1 kHz standard source by substituting a 100 kHz, low-pass current amplifier of known gain, for the amplifier shown in Fig.2.

The total scattered photon flux, eq.(1), is then used with a measurement of laser energy, I_o, (typically 4 joules at the input window) to evaluate the electron density. These scattering measurements are compared in Fig.10 with the density evaluated after Abel inversion from the phase shifts on a 2 mm μ-wave, multi-channel interferometer[9]. In the case illustrated the agreement between the interferometric density and the density from Thomson scattering is within 10%. Considering that the agreement is within the 15 to 20% errors of the two methods of measurement over the whole series of measurements it is probable that the fraction of any very high energy electrons is less than 10% of the total. Considerations of energy balance and of the agreement between the diamagnetic energy and the transverse energy from laser scattering restricts the number of high energy electrons ($> 10kT_e$) to less than a few per cent.

The absolute intensity of Balmer α was measured on the channels centred around 6563 Å simultaneously with the Thomson scattered spectrum. The number density of neutral hydrogen atoms, the electron density and temperature could thus be evaluated for the same locality in the torus. The particle confinement time and the charge-exchange losses were then evaluated as described in Section 13.

RESULTS

7. ELECTRON TEMPERATURE AND DENSITY DURING THE OHMIC HEATING PULSE

The sequence of figures from 10 to 17 summarise the results of the Thomson scattering measurements of electron temperature and density on the magnetic axis during the ohmic heating pulse.

The temperature rises to a maximum within about 15 ms from the start of the current and thereafter remains fairly constant throughout the current pulse duration. Apart from the initial spike, the density is similarly, slowly varying. Figs.10 and 11 refer to the long 70 ms current pulse shown in Fig.10(a). Figs.12 to 16 show the initial rise in temperature in more detail but refer to a shorter (35 to 40 ms) pulse (whose shape is shown in Fig.12). It should be noted that with the 35 ms pulse the current rises to a maximum in about 4 ms while the temperature rises more slowly. After 4 ms the current and the density are almost constant and during this period T_e rises to a maximum in about 8 ms. The rate of increase of the temperature can be estimated by balancing the resistive heating against the electron energy loss. A characteristic time to reach a stationary temperature is approximately equal to τ_E, the electrons being the main agency in the loss process (Section 17) and τ_E is the energy confinement time. Using the values of τ_E in table II (Section 17) it can be seen that the observed rise time is of this order.

By adjusting the vertical field pulse, the pressure and the timing of the separate capacitor banks, it is possible to produce a stable discharge with a second current increase as shown in Fig.17[20]. The current rises to an initial peak at 70 kA within 6 ms then reaches a second maximum of 105 kA after 16 ms. A significant rise in temperature on the axis is observed due to the second current step. The temperature on the axis now increases more rapidly than the current, in contrast to the temperature rise for a 'flat' current pulse shown for example in Fig.16.

8. SCALING OF ELECTRON TEMPERATURE WITH THE DISCHARGE PARAMETERS

Since the temperature varies with time throughout the current pulse, with radius and with the pulse shape, we will confine our remarks on scaling to the peak temperature on the magnetic axis and for ohmic heating currents which vary in time as illustrated in Fig.12.

The range of densities studied varied from 1×10^{13} cm^{-3} to 4.5×10^{13} cm^{-3} while peak currents from 40 kA to 145 kA were used with toroidal fields of up to 37 kOe. Figs.15 (lower) and 18 illustrate the variation of n_e and T_e with increasing current, up to and beyond the stability limit, for a constant initial gas pressure and stabilising field, B_o. This exemplifies the difficulty of holding one plasma parameter constant while varying the other parameters. The scaling of the temperature with density (holding I constant) can be appreciated from Fig.19, whilst Fig.20 shows the dependence on the heating current (holding n_e constant). It is evident that T_e scales as $n_e^{-\alpha}$ where α is approximately unity.

The dependence of T_e on ohmic heating current (Fig.20), for constant n_e, follows closely $T_e = \text{Const. } I^2$. No consistent dependence of the temperature on B_o, the main toroidal field, is observed from the Thomson scattering experiments.

The value of $n_e(o)\, T_e(o)$, the peak value of the product of density and temperature on the axis, is plotted in Fig.21 against I for almost all the conditions studied. It is evident again that there is no marked dependence of electron energy on B_o.

9. TEMPERATURE VARIATIONS WITH LARGE CURRENTS (> 100 kA)

As predicted by the above relation the highest temperature is recorded for the lowest density combined with the highest ohmic heating currents. In the present experiments a maximum T_e of 2 ± 0.35 keV was recorded with $n_e(o) = 1.8 \times 10^{13}$ cm^{-3} and I = 128 kA.

Under these conditions no neutrons were observed. However by increasing the density to above 3.5 10^{13} cm^{-3} and keeping the current high (> 120 kA), a detectable yield of neutrons is produced with T_e between 800 eV and 1.05 keV and with the ion temperature a maximum at 450 eV[2]. The highest values of $n_e(o)$ $T_e(o)$ shown in Fig.21 are from discharges with these plasma parameters.

10. UNSTABLE PLASMA CONDITIONS

The plasma column can be made unstable to long wavelength MHD instabilities by increasing the ohmic heating current and reducing the stabilising field, B_o, so that the margin for stability at the plasma boundary, q, falls below 2. The appearance of oscillations on B_θ pick-up coils is a sensitive test for instabilities[21] though as the amplitudes of the instabilities grow discontinuities are also observed on the voltage waveforms. Fig.22(a) illustrates the typical spikey voltage waveform observed in a mildly unstable plasma. The current has been increased over that given for the stable plasma condition shown in Fig.22(b). As the current falls later in time during the pulse the plasma column regains stability. The plasma temperature and density on the magnetic axis have been evaluated for these mildly unstable plasmas and it is apparent that the electron temperature does not decrease by more than 20% over that for a stable plasma with the same ohmic heating current and the same density. The voltage spikes and the accompanying modulation in the H_α intensity, shown in Fig.23, (which shows a rapid change (< 20 μs) in H_α correlated with a voltage spike, accompanied by a 3 kHz oscillation) are probably due to periodic excursions of the plasma to the limiter. Presumably energy is lost from the outer layers of the plasma only.

It is of interest to note that it is possible to have a stable discharge with q not more than 2 e.g. in the case of the stepped current waveform, Fig.17, the value of q at the plasma boundary was 2 in the middle of the pulse without any sign of instabilities or rapid energy loss.

11. RADIAL MEASUREMENTS OF n_e and T_e

The electron pressure profile in the vertical plane from the Thomson scattering measurements is compared on the same discharges with the results of the multi channel μ-wave interferometer (located on the opposite side of the torus) which recorded the density distribution in the horizontal plane. Thus the extent of the hot plasma and its radial and azimuthal symmetry could be evaluated.

The density and temperature vertically above and below the magnetic axis is shown in Fig.24 at 4 ms and at 18 ms (when the temperature reaches a maximum) from the initial current rise. Within the error of the measurement the plasma pressure is symmetrical in the vertical plane about the magnetic axis. In the horizontal plane the density profile is also symmetrical provided the vertical field current pulse is correctly shaped to give no inward or outward plasma drift.

Confining our attention now to only half of the vertical diameter, Figs.24, 25, 26 show that the density and temperature in the middle of the heating pulse are sensibly constant over ⅓ of the minor radius which is defined by the limiter (r_L = 17.5 cm). The plasma pressure is therefore flat over this central region, falling to half its peak value at about 12 cm from the axis.

A sequence of radial density and temperature measurements throughout the heating pulse is shown in Figs.26 and 27, in the case where the horizontal displacement of the plasma and current is less than 1 cm. It is evident that there is no gross radial shrinkage of the plasma column throughout the pulse.

These results are to be compared with the results shown in Figs.28, 29(a) and 29(b) which refer to discharges where the horizontal plasma drift becomes progressively large, reaching 7 cm near the end of the pulse. The electron pressure now falls off most steeply in the case when the plasma displacement is large. The outer 'hot' plasma boundary (arbitrarily defined to be plasma with $T_e > 50$ eV, the lower limit of the scattering measurements) corresponds in time with displacements in the interferometric density profile. This suggests that there is no appreciable body of cold electrons i.e. $n_e(r)\ T_e(r) < 0.03\ n_e(o)\ T_e(o)$ between the plasma boundary and the limiter, ($14 < r < 17.5$ cm).

The temperature profile on some discharges shows a modest increase over the central value due to resistive skin currents early in the discharge, i.e. 4 ms from current start. The magnitude of the temperature increase can be greater than the statistical errors (Section 6) and is evident for separate experimental runs shown in Figs.14(b), 26, 27. The skin temperature however is never more than 50% greater than the value on the magnetic axis.

In the middle of the current pulse the skin temperature has disappeared and the radial temperature profile is slightly flatter than parabolic following a relation

$$T_e = T_e(o)\left[1 - (r/a)^4\right]^2 \qquad \ldots (4)$$

Late in the current pulse (30 ms from current zero) the temperature profile is approximately parabolic.

Summaries of the radial temperature and density profiles from Thomson scattering for various times, throughout the discharge, are shown in Figs. 30 and 31 respectively. The separate symbols, each being the average of between 6 and 10 discharges, denote the results of different experimental runs, the points being normalised to the values on the magnetic axis.

The average density profile in the middle of the current pulse, Fig.31, is similar to the temperature profile and is in agreement with the interferometer observations of Gorbunov[9].

In order to evaluate the total electron energy in the plasma column it is convenient to calculate the mean radius $\bar{r}_p$ of the plasma pressure from the radial temperature and density profiles, viz,

$$2\pi \int_o^a r\, n_e(r)\, T_e(r)\, dr = \pi\, \bar{r}_p^{\,2}\, n_e(o)\, T_e(o) \qquad \ldots (5)$$

During the middle of the current pulse, $\bar{r}_p = 12$ cm.

It is of interest to evaluate the value of β_θ i.e. the ratio of the total kinetic pressure to the pressure of the magnetic field associated with the ohmic heating current, through the relation

$$I^2\, \beta_\theta = 200\, N\, k\, (T_e + T_i) \qquad \ldots (6)$$

where T_e and T_i are mean temperatures, and N is the line density, i.e. $\pi \bar{r}_p^2 \, n_e(o)$. The ion temperature is determined from the neutral particle emission[1]. Fig.32 shows that the value of β_θ is about 0.5 at the time of maximum temperature while late in the current pulse the value of β_θ can reach 2.

12. COMPARISON OF THE ELECTRON TEMPERATURE FROM THOMSON SCATTERING AND THE DIAMAGNETIC TEMPERATURE, T_D.

A comparison between the electrical measurements and the scattering measurements of the plasma energy is discussed fully elsewhere[11,12]. The total transverse energy, $E_\perp$, is calculated from the magnetic flux in the plasma column as described by Mirnov[19]. This diamagnetic signal shows that the plasma is paramagnetic initially and late in time it becomes diamagnetic, which is in agreement with our results for β_θ, Fig.32. The diamagnetic temperature T_D, is determined from the relation $T_D = \dfrac{E_\perp}{\pi r_I^2 \, \bar{n}_e}$ and therefore the accuracy is limited by the determination of the current radius, r_I, from the circuit equations.

Fig.33 shows the temporal variation of T_D with the mean electron temperature from laser scattering, $\overline{T_{eL}}$ estimated as described in Sec.11, for a typical set of experimental conditions. At most, T_D is a factor of 2 greater than $\overline{T_{eL}}$. However the ion temperature, T_i, must also be allowed for, and this was measured directly from the neutral particle energy spectrum. For the discharge illustrated in Fig.33, $\bar{T}_i$ = 220 eV and when this is added to $\overline{T_{eL}}$ then there is agreement within experimental error between the diamagnetic and laser-derived temperatures. The accuracy in estimating T_D is 30%, while for the laser measurement $\bar{T}_{eL}$ is accurate to within 15%.

In general, any large discrepancy between T_D and $\overline{T_{eL}} + \bar{T}_i$ can be ascribed to an underestimate of r_I (which may be partly due to non flux conservation of the vertical field) from a solution of the circuit equations. The increasing divergence between the laser and the electrical measurements in Fig.33 at late times in the discharge is due to the estimate of r_I falling well below 10 cm while the plasma radius, $\bar{r}_p$, remains fairly constant between 10 and 12 cm.

13. EXPERIMENTAL PARTICLE CONFINEMENT TIME

A balance between the particle loss rate and the injection and ionisation of neutrals into the plasma column can be written

$$- \frac{d\bar{n}_e}{dt} = \frac{\bar{n}_e}{\tau_n} - C \, I \, (H\alpha) \qquad \ldots (7)$$

where τ_n is the particle confinement time and C I (Hα) is the number of ionizing collisions per unit of time which is equal to the neutral particle influx, $\dfrac{dn_o}{dt}$. Following Kuznetsov[15,16,17], $\dfrac{dn_o}{dt}$ is proportional to the number of excitation events to the n = 3 level, and therefore to C I (Hα), where I (Hα) is the intensity of Hα and C is of the order of 4 for our plasma parameters (T_e > 100 eV and $n_e \simeq 10^{13}$ cm^{-3}). The intensity of Hα is measured simultaneously with the Thomson scattered spectrum on the channel centred on 6563 Å.

Fig.34 shows the intensity variation in time of the Hα radiation 25 ms after the current start. The light at earlier times has been occluded by the mechanical shutter and the apparent intensity modulation is due to shutter bounce. In the case of a stable plasma

the intensity decreases monotonically from the early spike (at about 2 msec) in the manner displayed in Fig.39(a).

A radial intensity plot of Hα, Fig.35, shows a peak near to the plasma boundary with a subsidiary peak outside the limiter. After Abel inversion, Fig.36, it is apparent that most of the Hα radiation comes from an annular source located about 13 cm from the magnetic axis and 2 to 3 cm wide. Since the ionization rate is practically independent of the plasma temperature above 50 eV, this implies that the neutral particles enter the plasma with a mean energy of about 1 eV. This may not be due to the production of energetic neutrals from absorbed gas but rather to the backscattered neutrals from the charged particle flux incident on the liner[18]. Figs.24, 37 and 38 illustrate that the Hα annulus tends to become more diffuse with time during the discharge.

Calculations of the particle loss time, τ_n, throughout the ohmic heating pulse are plotted in Figs.39 and 40 for two similar plasma conditions. The particle loss time reaches a maximum of 20 ms after peak current has been attained during the current pulse.

Figs.41 and 42 show the variation of the loss time with peak current and density, respectively. It is evident that the characteristic particle confinement time tends to rise with increasing current or average density, for stable conditions.

While it is recognised that the Hα analysis gives an over-estimate of the particle loss from the high temperature central core of the plasma, it is to be noted that particle loss from the plasma boundary is the relevant quantity in any assessment (see Sec.15) of the energy loss factor from the whole plasma column. The azimuthal (w.r.t. the major axis) variation of the loss has been measured on TM3 and although the intensity of Hα is higher near the limiter, an absolute measurement in any one cross section gives a reasonably accurate value for the particle confinement time of the plasma.

From the absolute flux of Hα the mean neutral particle density in the annulus near the plasma boundary is calculated to be 2×10^9 cm^{-3}. At the centre of the plasma this figure is ten times smaller. The energy loss time by charge exchange is therefore given by

$$\frac{1}{\tau_{ch\ ex}} = \frac{\int_0^a n_e(r)\, n_o(r) < \sigma\, v_i > T_i(r)\, r\, dr.}{\int_o^a n_e(r)\, T_i(r)\, r\, dr} \qquad \ldots (8)$$

which is of the order of 45 ms if we assume that the ion and electron temperature distributions are similar; σ is the charge exchange cross section and v_i the ion thermal speed.

14. SUMMARY OF EXPERIMENTAL RESULTS

The temperature rises to its maximum in about 15 ms after the start of the current pulse which is much slower than the risetime of the current. The maximum temperature observed is 2 keV at $n_e(o) = 1.8 \times 10^{13}$ cm^{-3} and with $I = 128$ kA. There is good agreement between the density measured by Thomson scattering and a microwave interferometer.

The temperature on the magnetic axis is practically independent of B_o but is approximately proportional to I^2 and to $(n_e)^{-1}$. Even under mildly unstable conditions i.e. at a margin of stability, $q = 2 \rightarrow 3$, the temperature on the axis does not fall by more than 20%.

The density and temperature distributions are symmetrical in the vertical plane. The radial temperature measurements show an initial slight increase in temperature at radii of 6 or 8 cm over the central values due to the existence of a skin current.

In the middle of the current pulse the radial temperature has a dependence

$$T_e(r) = T_e(o)(1 - (r/a)^4)^2 \qquad \ldots (9)$$

Late in the discharge when dI/dt is negative, the radial temperature distribution is parabolic.

The radial dependence of the density is similar to that of the temperature in the middle of the current pulse. The plasma pressure profile has a mean radius of about 12 cm, and does not shrink appreciably during the discharge.

In the discharges where there was a large horizontal displacement of the plasma column it was possible, by viewing at 16 cm from the axis, to observe the extreme outer edge of the plasma. No detectable body of cold plasma existed between the hot plasma and the limiter radius.

A step in the current pulse, designed to show heating in the outer plasma layers, resulted in a rapid increase of the temperature on axis; no outer skin temperature was observed.

Measurements of the neutral atom concentration from the absolute intensity of $H\alpha$ showed that the particle confinement time can reach 20 ms.

In the following sections these results are discussed.

DISCUSSION

15. THEORETICAL PARTICLE CONFINEMENT TIMES

The particle diffusion in a Tokamak is enhanced over that expected in cylindrical geometry by the Pfirsch-Schluter factor[23] and by trapped particle effects[8]. The form of the diffusion coefficient as a function of collision frequency is shown in Fig.43. The electron-ion collision frequency varies from $0.8 \rightarrow 4 \times 10^5$ s^{-1} over the range of parameters studied, whereas the lowest value for v_{th}/Rq was 1.0×10^6 s^{-1}, and $v_{th}/Rq \times (\frac{r}{R})^{3/2} \approx 0.6 \times 10^5$ s^{-1} ($r = 15$ cm and v_{th} is the thermal velocity of the electrons). Even allowing for an enhanced collision frequency due to anomalous resistivity we are always in the two trapped particle regions of Galeev and Sagdeev, except at the very outer edge of the plasma.

Thus

$$D_\perp = 2.6\, \nu_{ei} \frac{r_{ce}^2}{(r/R)^{3/2}} \cdot q^2 \qquad \left(\propto \frac{\beta_\theta}{\sigma}\left(\frac{r}{R}\right)^{1/2}\right) \qquad \ldots (10)$$

for $$\nu_{ei} < \frac{v_{th}}{Rq}\left(\frac{r}{R}\right)^{3/2} = \nu_1$$

and $$D_\perp = 1.25\sqrt{\pi}\, q \cdot \frac{r_{ce}}{R} \cdot \frac{cT_e}{eB_o} \qquad (\text{for } T_i \lesssim T_e, \text{ ref(29)}) \quad \left(\propto \frac{c}{R}\frac{T_e^{3/2}}{\quad}\right) \ldots (11)$$

for $$\nu_1 < \nu_{ei} < \frac{v_{th}}{Rq}$$

For our experiments $D_\perp$ in eq.(10) varies very little, since β_θ (Sec.20), and the effective conductivity (Sec.16) are approximately constant, whereas eq.(11) shows a $D_\perp$ increasing as the temperature increases. To make an absolute comparison between the values given by eq.(10) and the experimental values, we need to define carefully the particle confinement time in relation to a diffusion equation.

This equation is

$$\frac{dn_e(r)}{dt} = + \frac{1}{r}\frac{d}{dr} r D_\perp \frac{dn_e}{dr} + S(r) \qquad \ldots (12)$$

where S is the source of electrons due to ionization of neutral particles at the edge of the plasma. As $\frac{dn_e}{dt}$ is measured to be small, then the source and density profile are closely related, with $S(r)$ having the form shown in Fig.36. Experimentally we determine τ_n the particle confinement time as defined by Kuznetsov, from the relation

$$\tau_n = \frac{\bar{n}_e}{S_o - \frac{d\bar{n}_e}{dt}} \qquad \ldots (13)$$

$\bar{n}_e$ is the average electron density, and $S_o = \frac{dn_o}{dt} = S/V$ where S is the total number of injected electrons/s and V the equivalent volume over which the injection occurs. Experimentally $S(r)$ is found to be close to that associated with an annular ring of radius r_e and width δr_e emmiting the observed H_α line intensity.

The measured density profile at maximum current follows the relation $(1 - r^4/a^4)^2$ except near the region $r \approx a \approx 20$ cm, which corresponds to an $S(r)$ with a peak at about 13 cm, then $S_{max} = 8.65\, n_e(o) \frac{D_\perp}{a^2}$. If we identify this S_{max} with S_o then $\tau_n = \frac{a^2}{16.2 D_\perp}$ and this τ_n corresponds closely to the particle confinement time defined by $S_{max} = \frac{n_e\,(S_{max})}{\tau}$ or $\tau = \frac{a^2}{12.5 D_\perp}$. Using the Spitzer electron-ion collision frequency, but enhanced by an amount corresponding to the measured anomalous resistivity, ν_{eff}, we have compared the particle confinement times with those calculated from the eqs.(10) and (11) for average plasma parameters. The results are tabulated in Table I, which shows that the experimental containment times are all within a factor two or three of the theoretical times, if ν_{eff} is used. (N.B. ν_{eff} is always greater than $\nu_\perp$). Results obtained on TM3 are very similar[6].

TABLE I

Theoretical and Experimental Particle Confinement Times for Several Discharges

$\bar{n}$ 10^{13}	$\bar{T}_e$ eV	η_m/η_{cL}	ν_{eff} 10^5	q	$\nu_\perp = \frac{v_{th}}{R}(\frac{r}{R})^{3/2}$ 10^5	τ_n(theory) ms	τ_n(expt) ms
1.1	260	2.4	3.1	4	1.5	32	13
1.0	215	~ 1	1.5	6	0.9	28	18
1.0	215	2.5	3.8	4.6	1.2	36	12
0.9	190	~ 1	1.7	5.9	0.9	32	15.5
1.7	260	2.8	5.5	3.3	1.8	38	15
1.5	215	~ 1	2.3	5.9	0.9	29	19
1.7	280	1.8	3.2	3.1	2.0	36	15
1.75	305	2.05	3.3	3.1	2.1	32	16.5
2.2	255	1.25	3.3	3.3	1.8	39	20
1.5	220	1.9	4.3	3.7	1.4	45	23
1.2	122	1.0	4.3	6.8	0.6	57	18
1.5	220	3.6	8.2	3.7	1.4	46	15.5
1.5	435	6	4.8	2.1	3.7	28	-

It is worth noting that these observed containment times refer to the region where the neutral particles interact with the plasma, thus the containment time of a particle near the centre of the plasma may be much longer.

16. RESISTIVITY

Using the voltage and current waveforms together with the diamagnetic signal, the difference signal from two small magnetic coils to give the displacement of the current channel, and the vertical field, the inductance of the plasma column can be calculated and therefore its resistance. The resistivity, η_m, and conductivity temperature, $\bar{T}_{e\sigma}$, are then obtained using the calculated current radius. $\bar{T}_{e\sigma}$, as shown in Fig.33, is typical of many of our results which show that $\bar{T}_{e\sigma} < \bar{T}_{eL}$, with $\bar{T}_{e\sigma}$, after the initial current rise, fairly constant in the range 80 to 220 eV throughout the pulse.

In order to compare the resistivity η_m, with that expected classically, η_{cL}, it is convenient to define a resistive temperature, $\eta = C\,\overline{T_e^{3/2}}$, whence

$$\overline{T_e^{3/2}} = \frac{\int_0^a 2\pi\, r\, T^{3/2}\, dr}{\pi\, a^2} . \qquad \ldots (14)$$

The degree to which the resistivity is anomalous is given by $\overline{T_{eL}^{3/2}} \,/\, \overline{T_{e\sigma}}^{3/2} = \frac{\eta_m}{\eta_{cL}}$, where the subscripts m and cL refer to measured and classical. The anomalous factor varies throughout the pulse, being larger early in the discharge than at later times, viz. Fig.33. η_m/η_{cL} is anomalously high by up to a factor of 10 at the highest currents (> 100 kA) and lowest densities ($\sim 1.5 \times 10^{13}$ cm^{-3}) but approaches unity as the density is increased, Fig.44, and as the current decreases.

The plasma resistivity appears to behave therefore as in many devices (TM3, C-stellarator[7]) there being a critical value for the onset of the anomalous factor when the drift speed is close to the ion sound speed, i.e. $v_D/v_{iS} \simeq 1$ (where $v_{iS} = \sqrt{\frac{2kT_e}{m_i}}$ and the ion mass was not varied). The rate of increase of the anomalous character above this value appears to be faster than in TM3[5] and the spread of the results is large, Fig.45. In calculating the drift speed, the current radius is here defined as

$$\left[\frac{2}{T_e(o)^{3/2}} \int_0^a r\, T_e^{3/2}\,(r)\, dr\right]^{1/2} .$$

The calculated electrical resistivity should be corrected for the depletion of the current due to trapped particles (i.e. a factor $\simeq (1 + (r/R)^{1/2})$) and for collisions with impurities. The first factor may raise $\overline{T_{e\sigma}}$ by a few 10's of per cent only. The impurities cannot increase $\overline{T_{e\sigma}}$ by a large factor in the present device since bolometric measurements show the total radiation loss to be small. Corrections for finite electron Larmor radius effects are of the order only of a few per cent[7].

A dependence of the anomalous resistivity on the ratio of drift to sound speed, as shown in Fig.43, has been used to compute the current profile[14] and to show that there should be a strong skin effect even at temperature maximum ($\simeq$ 15 ms). A weak skin effect is observed and that only at early times. Anomalous electron heat conduction is therefore present with an effective heat diffusion coefficient exceeding that for anomalous

field diffusion. The calculations[14] also show that no skin effect in the temperature is to be expected at later times, when the current is reversed at the outer edge of the plasma. (The actual current distribution is not known.)

For the case of a current pulse with a second rise, Fig.17, the field diffusion time calculated from the measured resistance is such that a weak skin effect should have been observed. None was observed, again indicating anomalous electron thermal conductivity.

17. ENERGY AND HEAT LOSSES

Typical values of the energy confinement time, τ_E, are shown in Table II and as

TABLE II

Comparison of Energy Confinement and Equipartition Times for Various Discharge Conditions

t(ms)	τ_{eq}(ms)	$\frac{\tau_{eq}}{\lambda} \cdot \frac{T_e + T_i}{T_e - T_i}$ (ms)	τ_E(ms)
12	4·7	13	4·5
30	4·1	24	4·5
18	7·5	20	2·6
13	5·2	19	2·6
18	3·5	22	5·5
18	4·2	16	7·2
18	15	12	5·0
15	13	7	2·5
20	24	5·1	2·0

these are much smaller than the observed particle confinement times, then particle diffusion cannot account for the energy loss. When the plasma parameters are approximately stationary then the energy equations for the electrons and ions are

$$\frac{T_e + T_i}{\tau_E} = \frac{T_e - T_i}{\tau_{eq}} + \frac{T_e}{\tau_{He}} + \frac{T_e}{\tau_{pe}} + \frac{T_e}{\tau_{radn}}$$

$$\frac{T_e - T_i}{\tau_{eq}} = \frac{T_i}{\tau_{pi}} + \frac{T_i}{\tau_{Hi}} + \frac{T_i}{\tau_{ch.ex.}} \qquad \ldots (15)$$

where τ_E, eq, He, pe, radn, pi, Hi, ch.ex. are the respective times for energy confinement, equipartition, electron heat conduction losses, electron particle loss, radiation loss, ion particle loss, ion heat loss and charge exchange. For ambipolar diffusion $\tau_{pe} = \tau_{pi} = \tau_n$. The total radiation has been measured and corresponds to a negligible energy loss. For our neutral particle densities ($\sim 2 \times 10^9$ cm^{-3} in the annulus) the charge exchange time is about 45 ms. As the particle loss is not significant then we have

$$\frac{T_e + T_i}{\tau_E} \approx \frac{T_e}{\tau_{He}} + \frac{T_e - T_i}{\tau_{eq}} \qquad \text{and,}$$

$$\frac{T_e - T_i}{\tau_{eq}} \approx \frac{T_i}{\tau_{Hi}} \qquad \text{for the ions} \qquad \ldots (16)$$

The latter equation for the ion energy loss has been used by Artsimovich[4] to show that $T_i \propto \sqrt[3]{IB_o R^2 n}$. Using the expression for the ion thermal conductivity[8] we arrive at the equation

$$\tau_n = \tau_{Hi} \left(\frac{m_i}{m_e} \right)^{1/2} \left(\frac{T_i}{T_e} \right)^{3/2} \cdot \frac{T_e}{T_i + T_e} \cdot 1{\cdot}2 \qquad \ldots (17)$$

for the connection between the ion heat-loss time τ_{Hi} and the particle diffusion time, τ_n (for similar density and ion temperature profiles). When $T_i \approx T_e$, τ_{Hi} is of the order of 2-3 ms for the parameters of Table I, and ion heat conduction could be a very significant energy loss mechanism. At lower concentrations when $T_e > T_i$, τ_{Hi} approaches the particle lifetime of about 30 ms, and ion heat conduction is not a significant energy loss process since τ_{Hi} is then much longer than τ_E. As pointed out before[10], if the thermal isolation was only due to the ions then τ_E should be related to the energy transfer time given by $\tau_{eq} = 17\, T_e^{3/2}/n_e$, when the electron-ion interactions result from classical binary collisions. Such a dependence is not observed but this could partly be because the electron-ion interactions are not classical. However as Eq.(15) shows we have to compare $\tau_{eq}\, \lambda^{-1} \frac{T_e + T_i}{T_e - T_i}$ with τ_E, where λ is the degree to which the resistivity is anomalous, if we assume τ_{eq} involves an enhanced collision frequency. This comparison in shown in Table II, and in no case does the ion loss term exceed 40% of the total energy loss. Consequently the ions are not the principal source of energy loss and the main loss process is anomalous electron thermal conductivity except possibly at the very highest densities. Even allowing for an enhanced collision frequency the actual thermal conductivity must be an order of magnitude greater than the neo-classical value.

It is worth noting that Kadomtsev[13] has derived an expression for the anomalous thermal conductivity due to current-convective instabilities. This expression has the same magnitude and functional dependence as the neo-classical loss due to trapped particles in the intermediate region except that R^2 is replaced by $80\ a^2$ (and $80\ a^2 \approx R^2$). As the electrons and ions are subject to such a loss then the observed anomalous loss could be due to such an instability.

18. RADIAL TEMPERATURE PROFILE

From the considerations of the previous Section the equation governing the electron thermal conduction is

$$j^2/\sigma = -\frac{1}{r} \frac{d}{dr} K_e\, r \frac{dT_e}{dr} \qquad \ldots (18)$$

where j is the current density and σ the electrical conductivity. It is illuminating to consider the solutions of this equation and the relation between the electrical and thermal conductivity that it implies. The radial variation of the temperature near the outside boundary is only sensitive to the form of $K_e(r)$. Nearer the centre the current profile becomes more important. Fig.46 shows some solutions of this equation for various assumptions about $K_e(r)$. j^2 was chosen to be parabolic for the comparison but the curves are not sensitive to this assumption. If σ is classical ($\propto T_e^{3/2}$) and K_e is related to the thermal conductivity along a field line ($\propto T_e^{5/2}$), possibly due to a mechanism suggested by Rusbridge[26], then we obtain a flat temperature profile, curve I of Fig.46. For the cross field thermal conductivity ($\propto n_e^2/T_e^{1/2}$) and assuming $n_e(r) \propto T_e(r)$ we obtain curve II and for $K_e \approx$ constant, curve III which is approximately parabolic. The neo-classical thermal conductivity for the weak collisional intermediate region, and that of Kadomtsev, is $\propto n_e T_e^{3/2}$ and therefore gives the temperature profile of curve I. Convective

plasma losses have also been considered[26] and these give rise to gaussian shaped profiles, curve IV. The observed profile, curve V, is flatter than parabolic and near the outer boundary this implies that K_e is only a weak function of density or temperature (curve III).

The measured temperature distribution, if expanded in the following way

$$T_e(r) = T_e(o) + \frac{r^2}{a^2} T_e^1 + \frac{r^4}{a^4} T_e^2 + \ldots \qquad \ldots (19)$$

has the property that $T_e^1 \ll T_e^2$ which in turn requires j^2/σ to be peaked off axis from Eq.(18). This indicates the possible existence of a skin current even at long times ($\approx$ 15 ms) as predicted by numerical calculations[14].

The relation between the electrical and thermal conductivity from (18) must be of the form

$$\frac{K_e}{n} = \frac{A}{\beta_\theta \sigma} \qquad \ldots (20)$$

when we have used the definition of β_θ and A is a constant depending on the current and temperature profiles.

Thus the electron heat diffusion coefficient is proportional to $(\beta_\theta\, \sigma)^{-1}$. As $\beta_\theta \cong \frac{1}{2}$ when the plasma parameters are stationary then the heat loss depends only on the electrical conductivity and this also has a relatively weak dependence on the discharge parameters. The heat loss would decrease as $T_e^{3/2}$ if the conductivity were classical but in practice this not the case and it has a much weaker dependence. Such a heat diffusion coefficient would account for the rapid diffusion of the temperature profile early in time when β_θ is small.

19. THE CURRENT DENSITY PROFILE

The hydromagnetic stability of a TOKAMAK is dependent upon the field configuration though if β_θ is large enough (of order unity) the necessary condition for stability is that $q = \frac{rB_o}{RB_\theta} > 1$ everywhere[28]. In addition if the pressure profile is flat near the centre it is also necessary that $\frac{dq}{dr} > 0$ for small r[25]. If $\beta_\theta \ll 1$ then the stability is much more sensitive to the detailed form of the magnetic field configuration. From the known density and temperature profiles it is interesting to determine the current profile subject to various assumptions. Ohm's law along a field line is $j_\parallel = \sigma_\parallel E_\parallel$ and if we can also write $j_\perp = \sigma_\perp E_\perp$ (the paramagnetic model) then

$$j_z = \sigma_\parallel E_z \left(1 - \left(1 - \frac{\sigma_\perp}{\sigma_\parallel}\right) \frac{B_\theta^2}{B^2}\right) \approx \sigma_\parallel E_z \qquad \ldots (21)$$

$$j_\theta \cong j_z \frac{B_\theta}{B_o} \left(1 - \frac{\sigma_\perp}{\sigma_\parallel}\right)$$

as $\frac{B_\theta}{B_o} \ll 1$. When the azimuthal field is approximately constant in time and all skin effects have died away $E_z(r)$ = constant, and for a classical electrical conductivity this gives $j_z(r) \propto T_e^{3/2}(r)$, $j_\theta(r) \propto T_e^{3/2}(r) B_\theta(r)$. Inserting the known temperature profile at a time when the above assumptions hold we obtain

$$j_z(r) = j_z(o)(1 - r^4/a^4)^3, \quad j_\theta(r) = \frac{j_z(r)}{B_o} \left(1 - \frac{\sigma_\perp}{\sigma_\parallel}\right) \frac{j_z(o)}{2} \left(1 - \frac{r^4}{a^4} + \frac{3}{5}\frac{r^8}{a^8} - \frac{1}{7}\frac{r^{12}}{a^{12}}\right) r$$

Assuming B_o to be approximately uniform this gives the critical $q(a) = 2{\cdot}2$, for q to be greater than unity on axis and therefore everywhere. The value of $q(a)$ necessary experimentally is usually close to this number.

However, the electrical conductivity near current maximum is never classical and has a value lying somewhere on the curve of Fig.45, which we can express in the form

$$\sigma_{\parallel} = \sigma_{Cl}\left(1 + \lambda\left(\frac{v_D}{v_{iS}} - 1\right)^2\right),$$

for $$\frac{v_D}{v_{is}} > 1,$$

where σ_{Cl} is the Spitzer value for the conductivity and λ is a constant. In this case for a uniform E_z we obtain $j_z(r) \propto \frac{n^2(r)}{T_e^{\frac{1}{2}}(r)} \propto \left(1 - \frac{r^4}{a^4}\right)^3$, as $n_e(r) \propto Te(r)$ experimentally, which is the identical result to the classical case.

Impurities, neutral and trapped particles all tend to lower the conductivity near the outside edge of the plasma and consequently the current is lowered in these regions. The current distributions are shown in Fig.47.

From pressure balance we have

$$\frac{dp}{dr} = -\frac{\sigma_{\perp}}{\sigma_{\parallel}} \frac{j_z B_\theta}{1 - \left(1 - \frac{\sigma_{\perp}}{\sigma_{\parallel}}\right)\frac{B_\theta^2}{B^2}} \approx -\frac{\sigma_{\perp}}{\sigma_{\parallel}} j_z B_\theta \qquad \ldots (22)$$

and integrating we obtain

$$\beta_\theta I^2 = 2Nk(T_e + T_i), \quad \beta_\theta = \sigma_{\perp}/\sigma_{\parallel} \qquad \ldots (23)$$

The classical value for β_θ is therefore $\frac{1}{2}$ which is always observed (Sec.20).

At earlier and later times E_z is not uniform and the above arguments are not valid. However sufficiently late in time $\beta_\theta \approx 1$, then B_o must be approximately uniform so that the pressure balance equation takes the simple form

$$-\frac{dp}{dr} = B_\theta\, j_z \qquad \ldots (24)$$

The measured electron pressure profile at such times is $\propto (1 - r^2/a^2)^2$ and consequently $j_z(r) \propto (1 - r^2/a^2)/(1 - \frac{2}{3}\frac{r^2}{a^2})^{\frac{1}{2}}$ if we assume the ion pressure profile to be similar. Again the current profile is not very different from the temperature profile.

At later times the effective current radius deduced from the electron temperature profile is a little smaller than at current maximum but not by a factor as large as that deduced from inductance measurements. This shrinkage has been postulated as due to a pinch effect associated with the trapped electrons[30] at a velocity $\sim E_z/B_\theta \sim 2 \times 10^3$ cm s^{-1} but the observed shrinkage ($\approx 2 \times 10^2$ cms^{-1}) is much less than this velocity would indicate.

(It has been shown by Shafranov[28] that a current radius somewhat smaller than the plasma radius is necessary for stability to a finite resistive tearing mode with azimuthal mode number 2, however no such slow growing instability is observed though the current and plasma radius appear to be not very different.)

20. DISCUSSION OF β_θ

Our observed scaling law that $n_eT_e \propto I^2$ can be related to the simple Bennett

relation $\beta_\theta I^2 = 2\,NkT$ if we calculate the average electron and ion energy. The latter is obtained from neutral particle measurements, and in those cases where T_i was not measured, by interpolation from the formulae $T_i \propto \sqrt[3]{I\ n\ B_o R^2}$. The results are shown in Fig.48, where we have also compared the results obtained by the diamagnetic measurements. The mean value of β_θ when the plasma parameters are stationary (i.e. there is no increase in heating) is $0{\cdot}47 \pm 0{\cdot}02$. Provided the plasma is stable this value is independent of the current, stabilising field and density over the range of these parameters studied.

The value of β_θ can be limited either by equilibrium, stability or diffusion. The observed values are still well below the possible equilbrium limit for a TOKAMAK ($\sim R/a$), and as no rapid MHD instabilities are observed β_θ must also be below the stability limit. The limiting β_θ is therefore determined by the loss process.

As already noted (Sec.19), $\beta_\theta = \frac{1}{2}$ is the result to be expected from a paramagnetic model if $\sigma_\perp/\sigma_\parallel = \frac{1}{2}$. This latter value is the classical result when the Hall current is not allowed to flow.

If the loss processes are neo-classical then the energy confinement time, or heating rate must be equal to the neo-classical containment time.

From Fig.43, for the Pfirsch-Schluter regime we have

$$\frac{N(\overline{T_e + T_i})\pi\, a^2}{I^2}\,\sigma_\parallel \approx \frac{\sigma_\parallel\, a^2}{\beta q^2} \qquad \ldots (25)$$

and hence $\beta_\theta \approx \frac{R}{r}$ (which is similar to the quoted 'equilibrium' limit in a TOKAMAK). In the collision-free region of Galeev and Sagdeev, a similar balance gives

$$\beta_\theta \approx \left(\frac{R}{r}\right)^{\frac{1}{4}} \qquad \ldots (26)$$

which is a number only a little greater than unity (1·6 for T3). Most of the experimental results lie in the weak collisional intermediate region where we find

$$\beta_\theta \approx \left(\frac{R}{r}\right)^{\frac{1}{4}} \left(\frac{\nu}{\nu_1}\right)^{\frac{1}{2}} \qquad \ldots (27)$$

which for our data can have values of up to 3.

The observed value of $\beta_\theta = \frac{1}{2}$ at temperature maximum is evidently the result of an anomalous loss process associated with electron thermal conduction. This value is also predicted on the basis of the paramagnetic model for the classical ratio of $\sigma_\perp/\sigma_\parallel = \frac{1}{2}$. The value of β_θ observed late in the current pulse may be due to the fact that the loss processes become neo-classical and we approach the limit set by Eq.(27). It could also be due to the energy content of the discharge responding to the decreasing current with a time delay of the order of the energy confinement time. Nevertheless the plasma showed no signs of reaching an equilibrium or stability limit.

In addition to these limits on β_θ for an ohmically heated system there is also one interesting point associated with the net drift inwards of trapped particles[30] which produces a current

$$\approx n_e \left(\frac{r}{R}\right)^{\frac{1}{2}} \frac{E_z}{B_\theta}$$

compared with the outward current due to diffusion

$$\approx \frac{\beta\theta}{a\sigma_{\parallel}} \left(\frac{r}{R}\right)^{\frac{1}{2}} n_e \cdot$$

Writing $j_z = \frac{1}{r}\frac{d}{dr} r B_\theta \cong \sigma_{\parallel} E_z$ we see that these two rates are comparable when $\beta_\theta \approx 1$, though for our parameters this number will be greater than unity as $\nu > \nu_1$. On this basis one would expect an inward drift of the plasma early in time when β_θ is small and an outward drift later in time. The expected drift of about 1 cm ms^{-1} is not observed, though such an effect could be masked by the relatively rapid energy loss processes. Late in time when a drift outwards of the same magnitude is expected, the confinement is good, and there is no expansion outwards.

21. SUMMARY

1. The distribution function of the electron velocities perpendicular to the major circumference has been measured by Thomson scattering and is close to Maxwellian. The density obtained from the absolute scattering cross section is in agreement with the density measured by a microwave interferometer.

2. Electron temperatures of 100 eV to 2 keV and densities of $1 \rightarrow 4{\cdot}5 \times 10^{13}$ cm^{-3} have been measured on TOKAMAK T3A.

3. The temperature and density profiles at the temperature maximum are flat over one third of the limiter radius and satisfy the relation $T_e(r) = T_e(o)\ (1 - (r/a)^4)^2$. Towards the end of the pulse they become more parabolic. The density profiles agree with those obtained from the multi-channel microwave interferometer. At early times there is a weak temperature maxima off axis due to skin currents.

4. There is good agreement between the diamagnetic plasma energy and the energy derived from the pressure profile obtained from scattering and ion temperature measurements; up to times of about 20 ms. When the diamagnetic temperature agrees with the sum of the electron and ion temperatures, the current radius, inferred from inductance measurements, is close to the pressure radius.

5. For parameter values at temperature maximum, the following scaling laws hold

1. I = const. $\quad T_e \propto \frac{1}{n_e}$
2. n_e = const. $\quad T_e \propto I^2$
3. $\quad n_e T_e \propto I^2$

No dependence on the value of the stabilising field was found provided that q was greater than 2-3 for stability.

6. The total energy content at temperature maximum scales as the square of the current and satisfies the modified Bennett relation

$$\beta_\theta I^2 = 2\,Nk(T_e + T_i)$$

with $\beta_\theta = 0{\cdot}5$. This value increases with time and reaches 2, which is close to the limit imposed by neo-classical diffusion (Sec.20), towards the end of the current pulse.

7. The observation that there is only a weak skin in the temperature profile during the current rise and none at all during the stepped current pulse regime can only be explained if electron thermal conductivity is anomalous.

8. Values for the particle confinement time deduced from absolute measurements of the

intensity of $H\alpha$ arising from an annular ring around the plasma are close to those predicted by Galeev and Sagdeev when an effective collision frequency is used.

9. The resistivity is always observed to be anomalous and increases rapidly when the ratio of drift to sound speeds exceeds unity. Only late in the current pulse does the resistivity approach its classical value.

10. Weak instabilities, sometimes observed when the safety factor q is in the range $2 \rightarrow 3$ do not affect the value of the temperature on axis. If q is 2 or below then 'instabilities' are observed which grow in less than 20 μs and are also associated with low frequency oscillations of the plasma column.

11. Using Ohm's law and pressure balance we find that the current profile at and beyond temperature maximum probably differs very little from the observed temperature profile.

12. The principal energy loss mechanism is identified as electron heat conduction except possibly at the highest densities where the ion thermal conduction may play a significant role.

22. ACKNOWLEDGEMENTS

The work presented in this report is based on the photon scattering measurements in a collaborative series of experiments during 1969 between the toroidal pinch group at Culham and the Tokamak group at the Kurchatov Institute.

The correctness of the analysis and the conclusions presented herein are the sole responsibility of the authors. However, the authors acknowledge that their ideas on Tokamak have benefited from many rewarding discussions with their Russian and British colleagues. In addition a necessary qualification for the success of the experimental programme has been the close and unstinted cooperation of the T3-Tokamak operating team.

The authors would like to thank Academician L.A. Artsimovich for his initial invitation to us to perform the photon scattering measurements, and to both Dr R.S. Pease and Academician L.A. Artsimovich for the stimulus of their continuous interest and for the benefit of their constructive criticism.

REFERENCES

1. AFROSIMOV, V.V., PETROV, M.P., (1967), Zh. T. Fiz., 37 11, 1995.
2. ARTSIMOVICH, L.A., ANASHIN, A.M., et al., (1969), Zh. E.T.F. Letters, 10, 130-133.
3. ARTSIMOVICH, L.A., BROBROVSKII, G.A., GORBUNOV, E.P. et al., (1968), Proc. 3rd Int. Conf. on Controlled Fusion, Novosibirsk, Publ. I.A.E.A., Vienna, Vol.1, p.157.
4. ARTSIMOVICH, L.A., GLUKOV, A.V. PETROV, M.V., (1970), JETP, Letters, 11, 449.
5. BOBROVSKII, G.A., KISLYAKOV, A.I. et al., (1969), Kurchatov Inst. Report, IAE-1905
6. BOBROVSKII, G.A., KUZNETSOV, E.I., RASUMOVA, K.A., (1969), Kurchatov Inst. Report, IAE-1906.
7. COPPI, B., MAZZACATO, E., Princeton Report, (1969), MATT-720.
8. GALEEV, A.A., SAGDEEV, R.Z., (1967), Doklady Akad. Nauk, 189, 1204.
9. GORBUNOV, E.P., DNESTROVSKII, V.N., KOSTOMAROV, D.P., (1968), Plasma Diagnostics, Issue 2, 188 Atomizdat, Moscow, 1968.
10. GORBUNOV, E.P., MIRNOV, S.V., STRELKOV, V.S. (1970), Nuclear Fusion 10, 43-51.
11. GORBUNOV, E.P., et al., Paper submitted to Rome Conference, September 1970.
12. GORBUNOV, E.P. et al., Paper submitted to J.E.T.P.
13. KADOMTSEV, B.B., POGUTSE, O.P., (1967), Questions on Plasma Theory, 5, 326. Atomizdat, Moscow.
14. KOSTOMOROV, D.P., DNESTROVSKI, Y.N., (1969), Conference on Toroidal Confinement Systems, Dubna, October 1969.
15. KUZNETSOV, E.I. (1968), Kurchatov Inst. Report, IAE-1636.
16. KUZNETSOV, E.I., VINOGRADOVA, N.D., (1968), Zh.E.T.F. Letters, 8, (2), 59-63.
17. KUZNETSOV, E.I., (1967), Zh.Tek. Fiz., 37, 1550.
18. McCRACKEN, G.M. Private Communication.
19. MIRNOV, S.V. (1969), Atomnaya Energiya, 26, 458.
20. MIRNOV, S.V. (1969), Nuclear Fusion, 9, 57-66.
21. MIRNOV, S.V., (1969), Kurchatov Inst. Report, IAE-1907.
22. PEACOCK, N.J., ROBINSON, D.C., FORREST, M.J., WILCOCK, P.D. and SANNIKOV, V.V., (1969), Nature, 224, 488-490.
23. PFIRSCH, D., SCHLUTER, A., (1962), Max-Planck Inst. Report, MP1/PA/7/62.
24. RHOR, H., (1969), Z. Physik, 225, 494-502.
25. ROBINSON, D.C. Conference on Toroidal Confinement Systems, Dubna, October, 1969.
26. RUSBRIDGE, M.G. Plasma Physics, (1969), 11, 35.
27. SCHEGLOV, J.A. (1967), Jh.E.T.F. Letters, 6, 11, 949-951.
28. SHAFRANOV, V.D. (1970), Zh. Tek. Fiz., 40, 241.
29. STRINGER, T.E., (1969), Phys. Rev. Letters, 22, 770.
30. WARE, A.A. (1970) Paper submitted to Phys. Rev. Letters.

Thomson scattering signals 6 cm from axis, 25 msec from start of current.

$[T_e = 640\,eV,\ n_e = 1{\cdot}4 \times 10^{13}\,cm^{-3},\ B_o = 17\,kG\ \hat{I}_z = 62\,kA,\ \tau = 70\,msec.]$

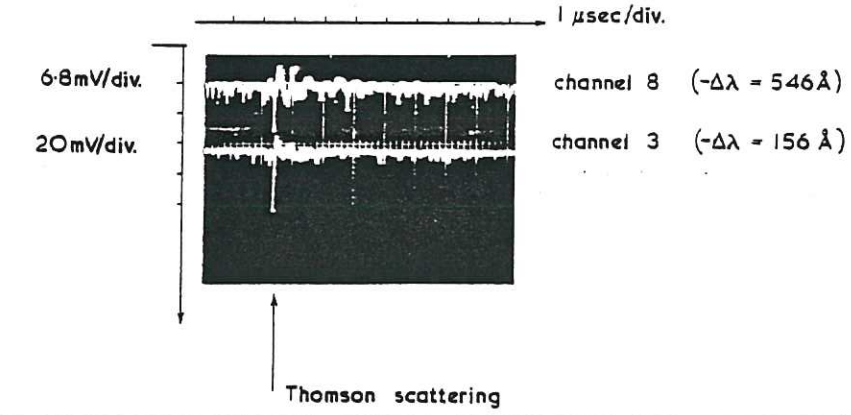

$[n_e(o) = 1{\cdot}7 \times 10^{13}cm^{-3}, B_o = 25\ kOe\ I = 90\,kA,\ \tau = 40\,msec]$

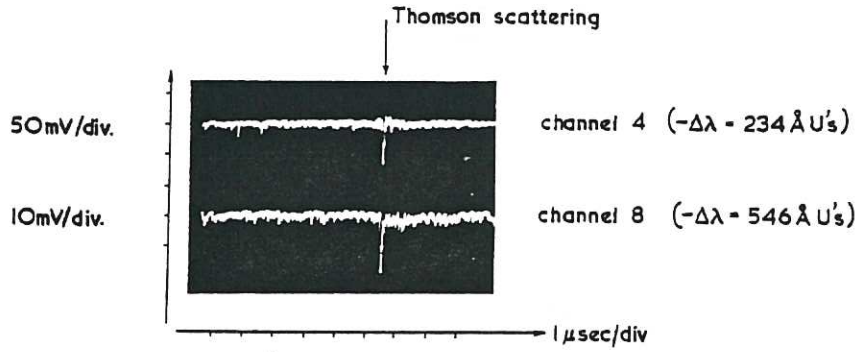

Fig.7 Thomson scattering on two detection channels, 20 msec from the start of the current pulse. A good signal to noise ratio is evident.
$n_e(o)$ is the density on the magnetic axis and τ is the current pulse duration.

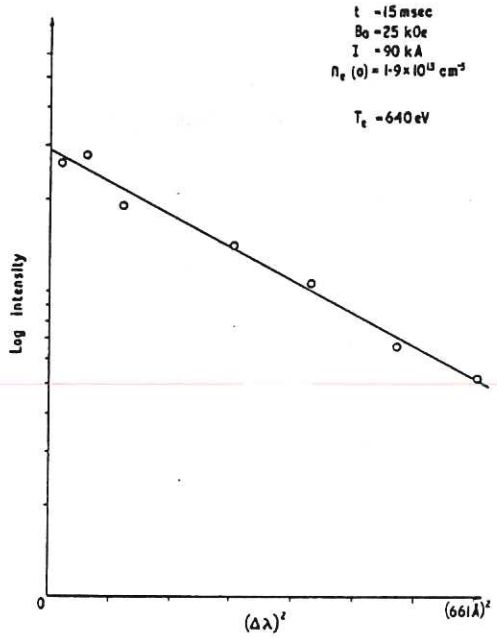

Fig.8 Logarithm of the scattered intensity as a function of the square of the wavelength displacement, $(\Delta\lambda)^2$. The linear behaviour is good evidence for the Maxwellian distribution of velocities transverse to the main field direction. The temperature in this case is 640 eV.

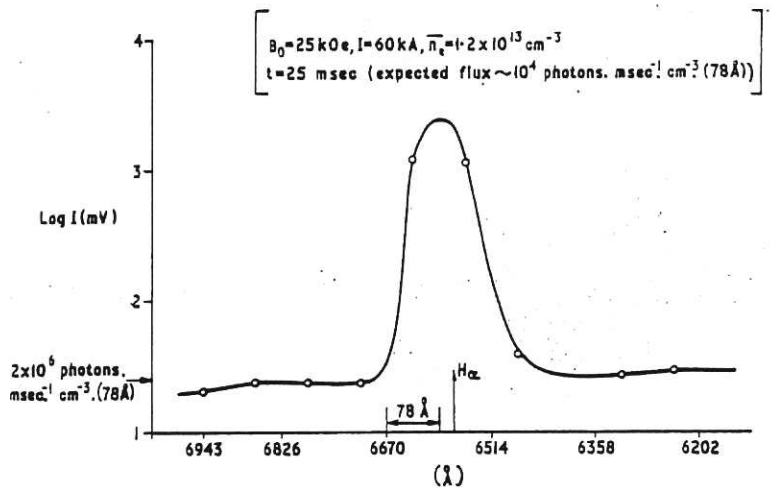

Fig.4 The spectrum of background radiation over the range of scattering wavelengths, showing the peak due to the Balmer α line. The channel width is indicated on the abscissae.

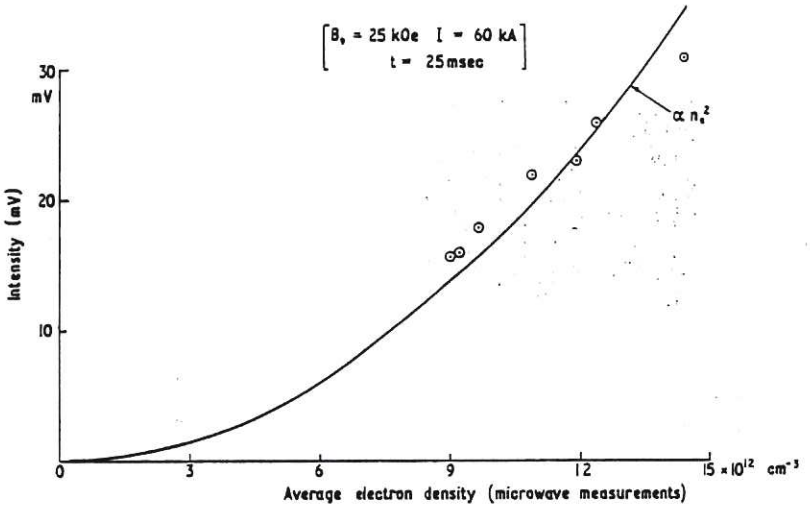

Fig.5 Intensity of background radiation as a function of average electron density. Full curve shows a quadratic dependence on the electron density.

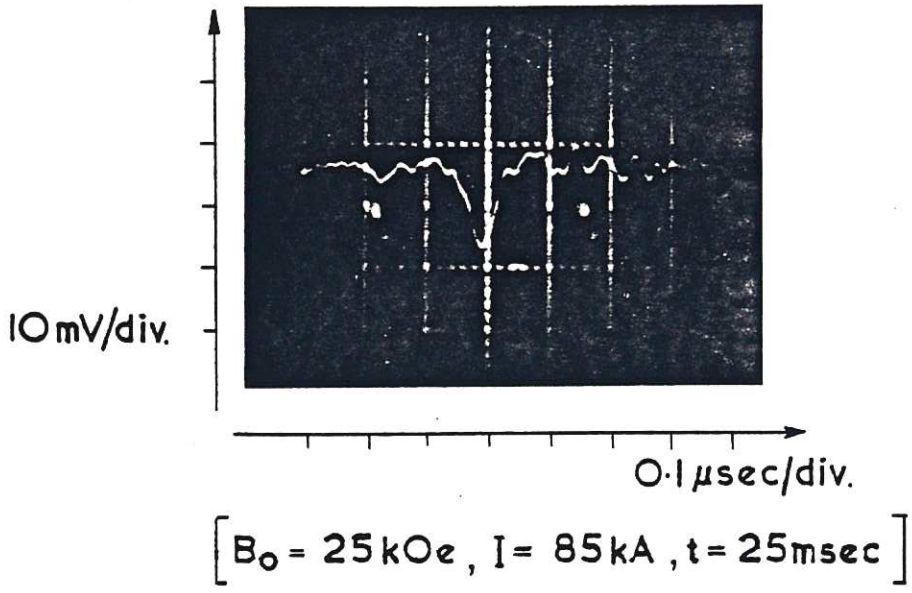

Fig.6 The scattered light signal displaced minus 468Å units from the laser wavelength, as a function of time. Half width after amplification and recording ≈ 40 nsecs.

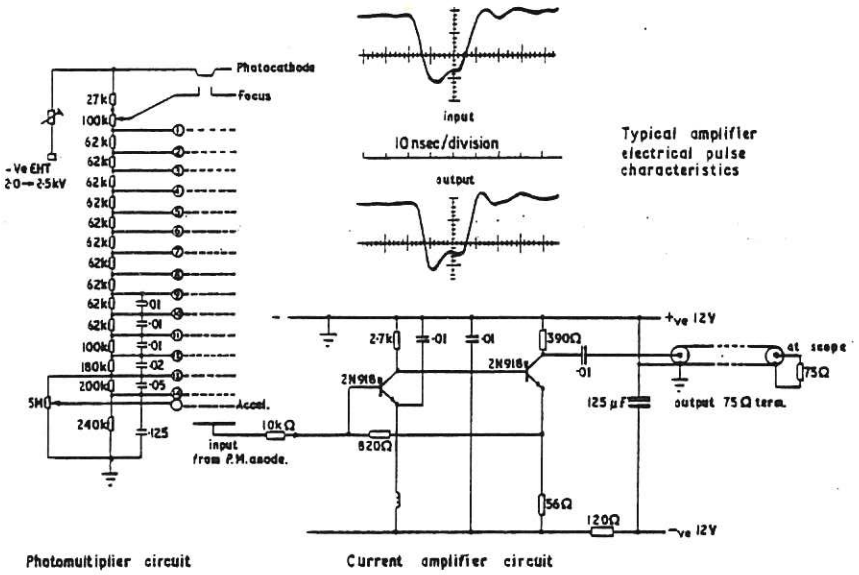

Fig.2 Photomultiplier and amplifier circuits used to detect the scattered photons.

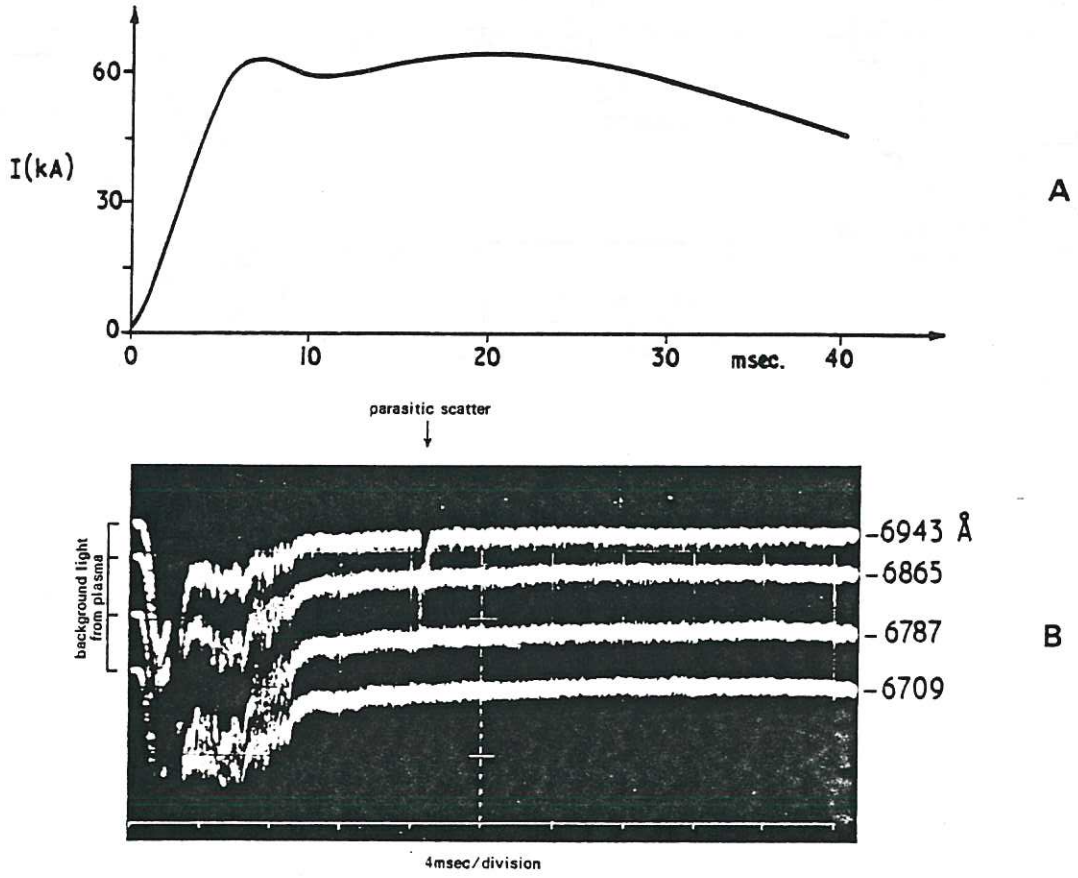

Fig.3 (a) Plasma current as a function of time.
(b) Temporal variation of the background light together with the parasitic scatter from relaxation mode operation of the laser. CLM-R 107

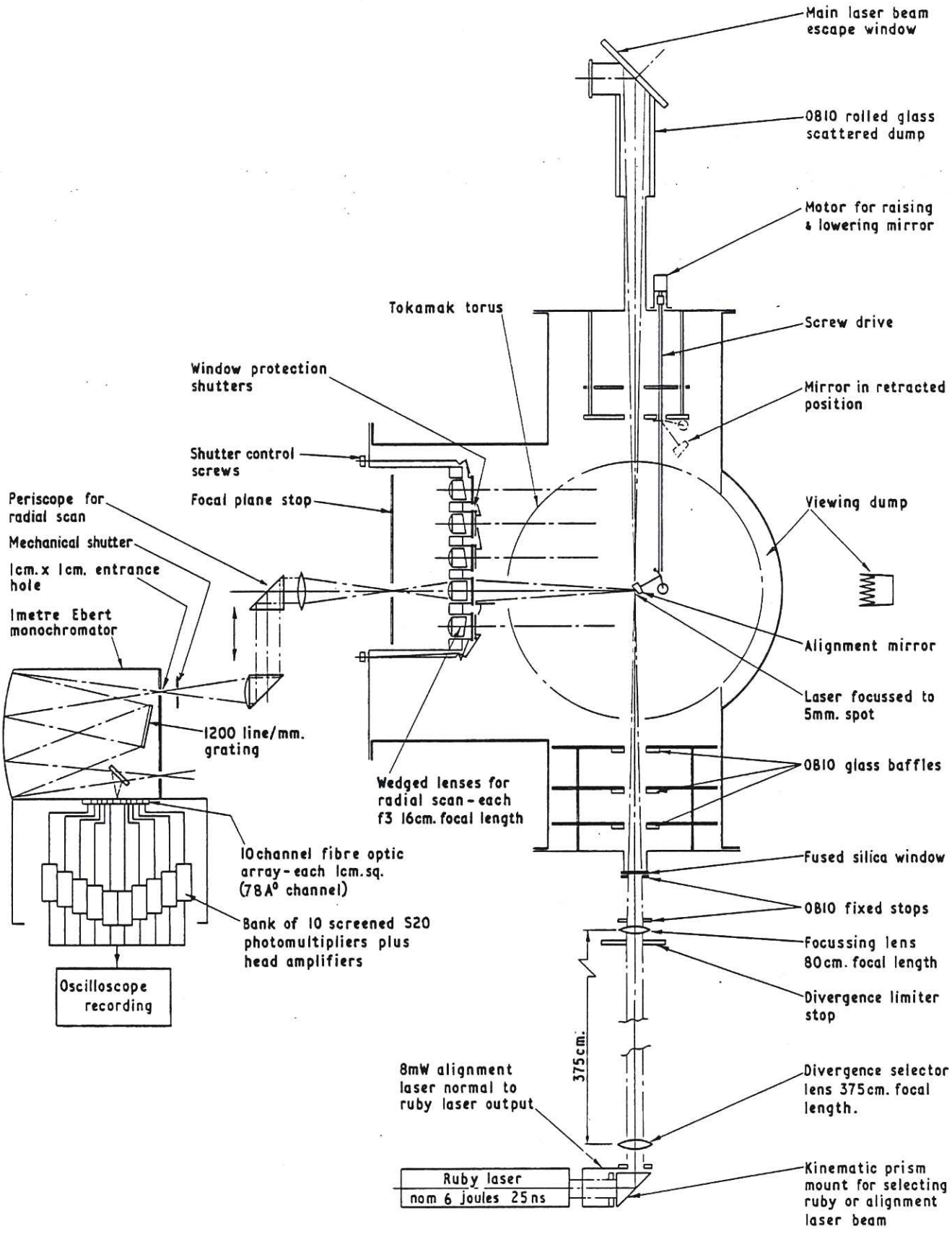

Fig.1 Schematic diagram of the laser scattering experiment on TOKAMAK T3

CLM - R 107

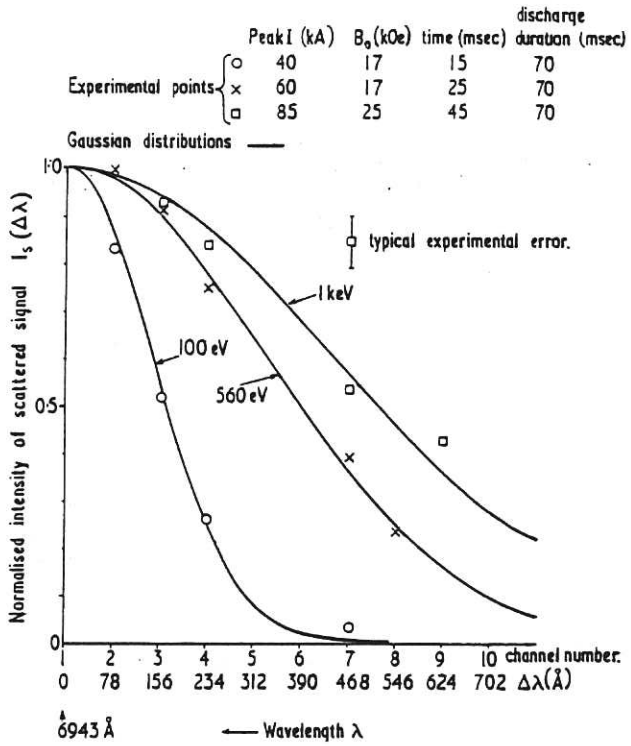

Fig.9 The scattered light spectrum for various discharge conditions, showing temperatures in the range 100–1000 eV.

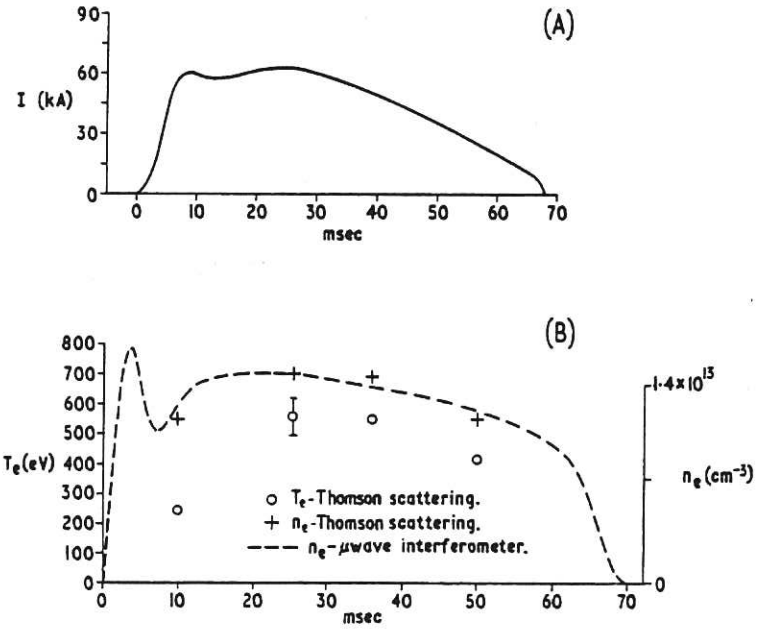

Fig.10 (a) plasma current as a function time.
(b) electron temperature and density as a function of time on axis. For comparison the central value of the electron density, obtained using a multi-channel microwave interferometer, is shown. The main stabilizing field was 17 kOe. CLM-R 107

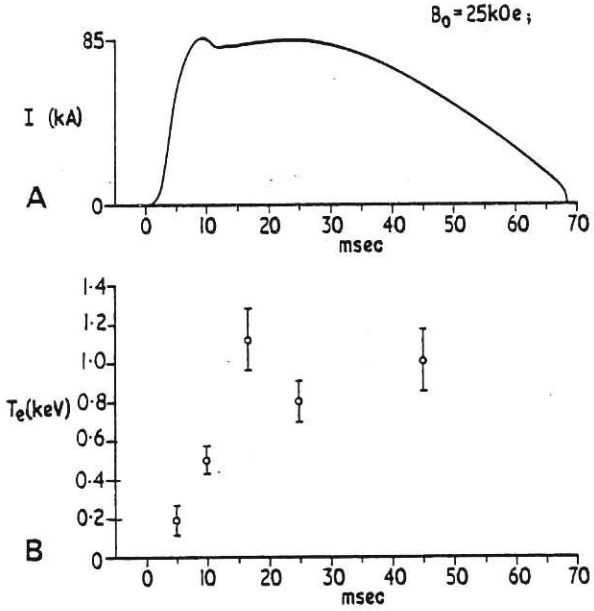

Fig.11 (a) Plasma current and (b) electron temperature as a function of time for an electron density on the axis of $1{\cdot}5 \times 10^{13}$ cm^{-3} at 25 msecs. Pulse duration 70 msecs.

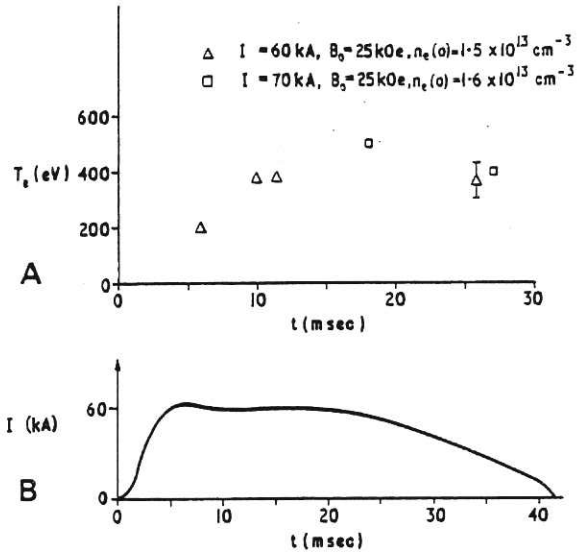

Fig.12 (a) Electron temperature and (b) plasma current as a function of time for a pulse duration of 40 msecs.

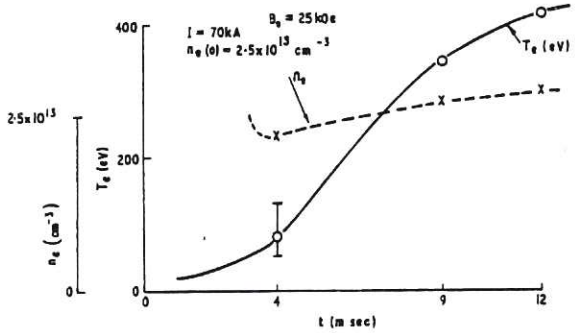

Fig.13 Electron density and temperature for early times during a current pulse. The electron density at 2 msecs, from microwave measurements, is much higher than that shown at 4 msec. Due to rapid changes in the density at about 4 msec considerable variation in the temperature can be experienced for nominally the same discharge parameters.

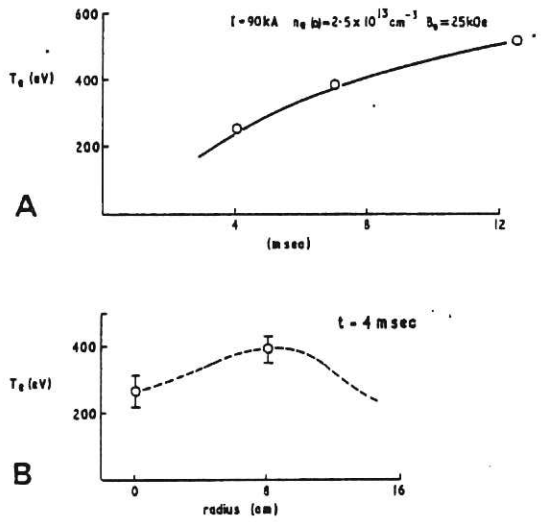

Fig.14 (a) Electron temperature at early times, and (b) observation of a weak skin effect at 4msecs from the start of the current pulse. CLM-R 107

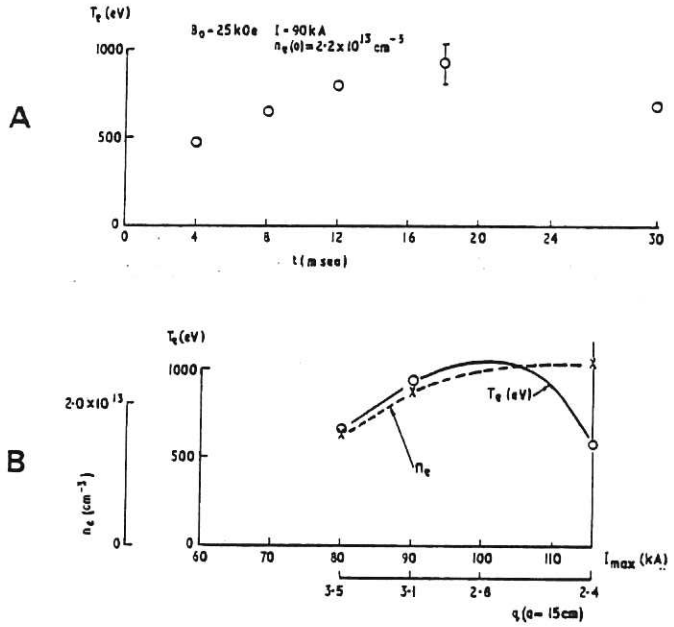

Fig.15 (a) temporal variation of the electron temperature for a plasma current of 90 kA, and (b) the variation of density and temperature (at t = 18 msec) with increasing current up to and beyond the stability limit. Values for the safety factor, q, calculated using a current radius of of 15 cms, are indicated. A discontinuity in the current was observed at 116 kA, due to plasma instability.

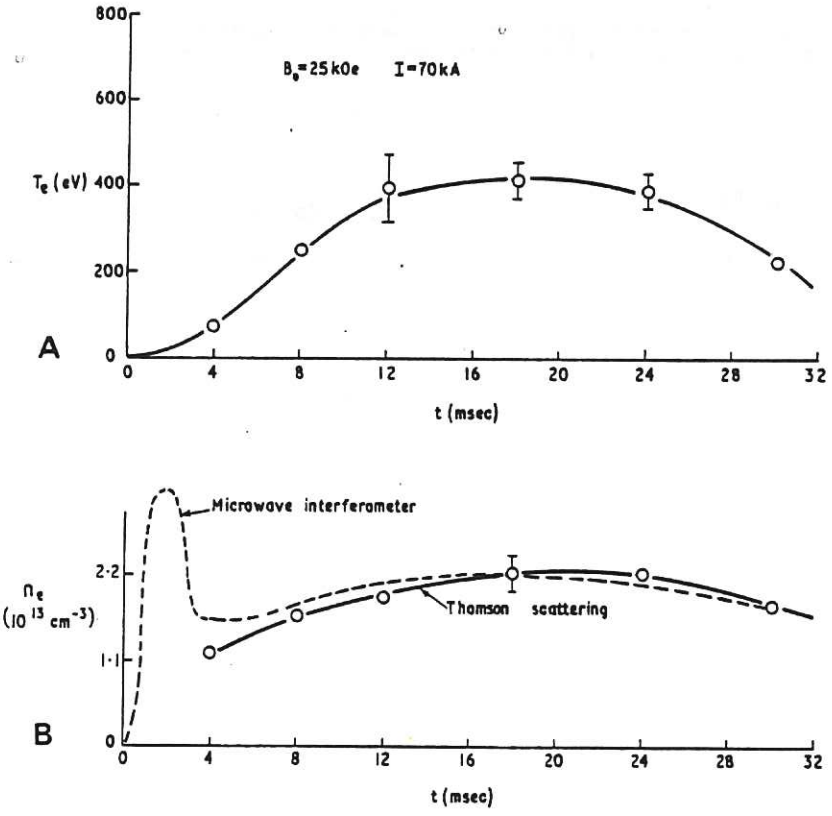

Fig.16 (a) Electron temperature and (b) density as a function of time through a current pulse from Thomson scattering. The density is compared with the interferometer measurements.

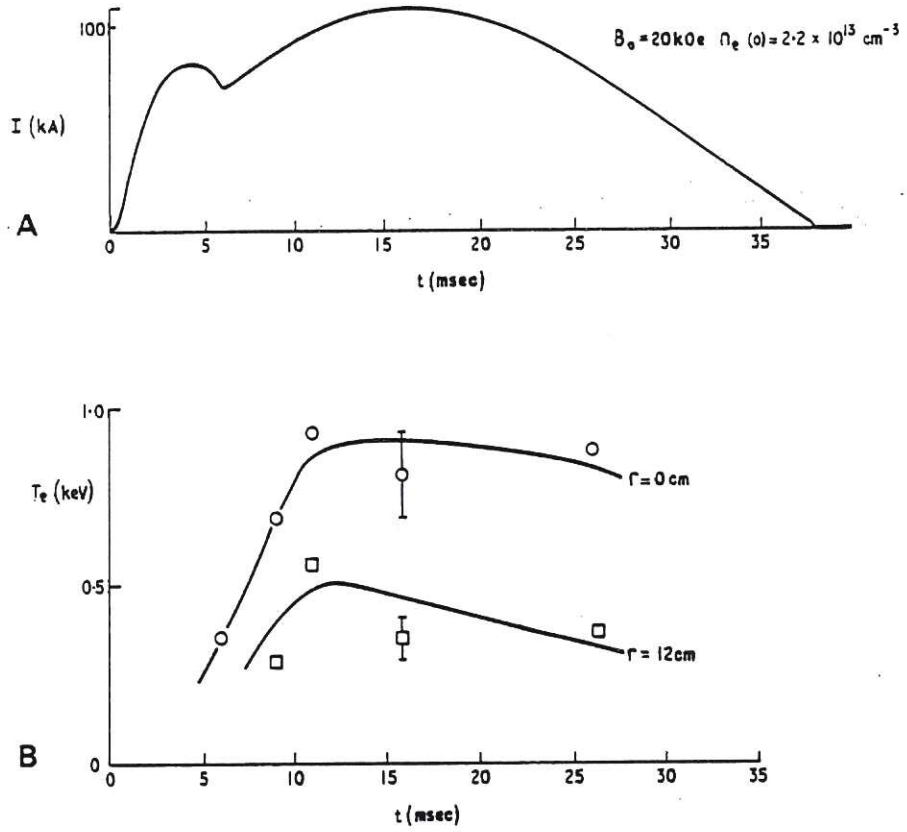

Fig.17 (a) Stepped current pulse and (b) electron temperature on and off axis (0 and 12 cms) as a function of time.

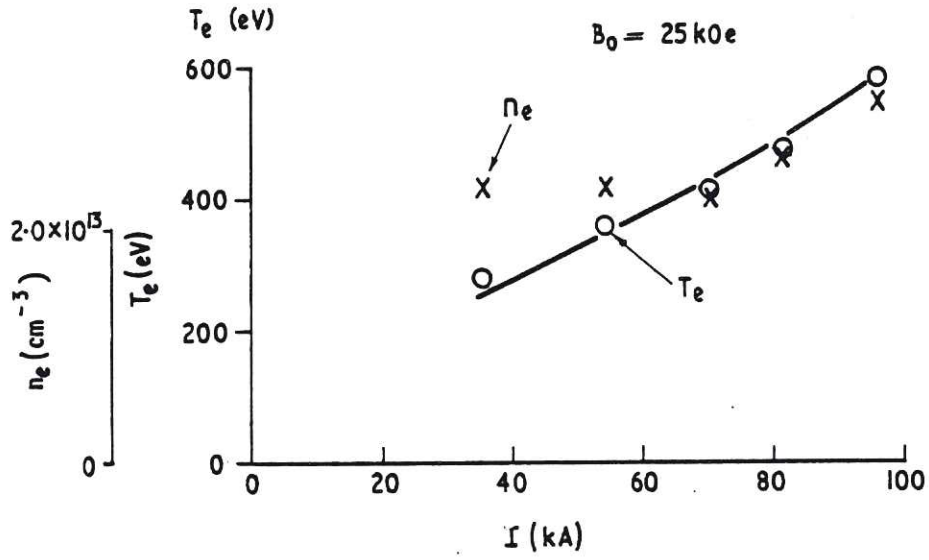

Fig.18 Electron density and maximum temperature as a function of the peak plasma current. Weak instabilities were evident at the highest current.

CLM-R 107

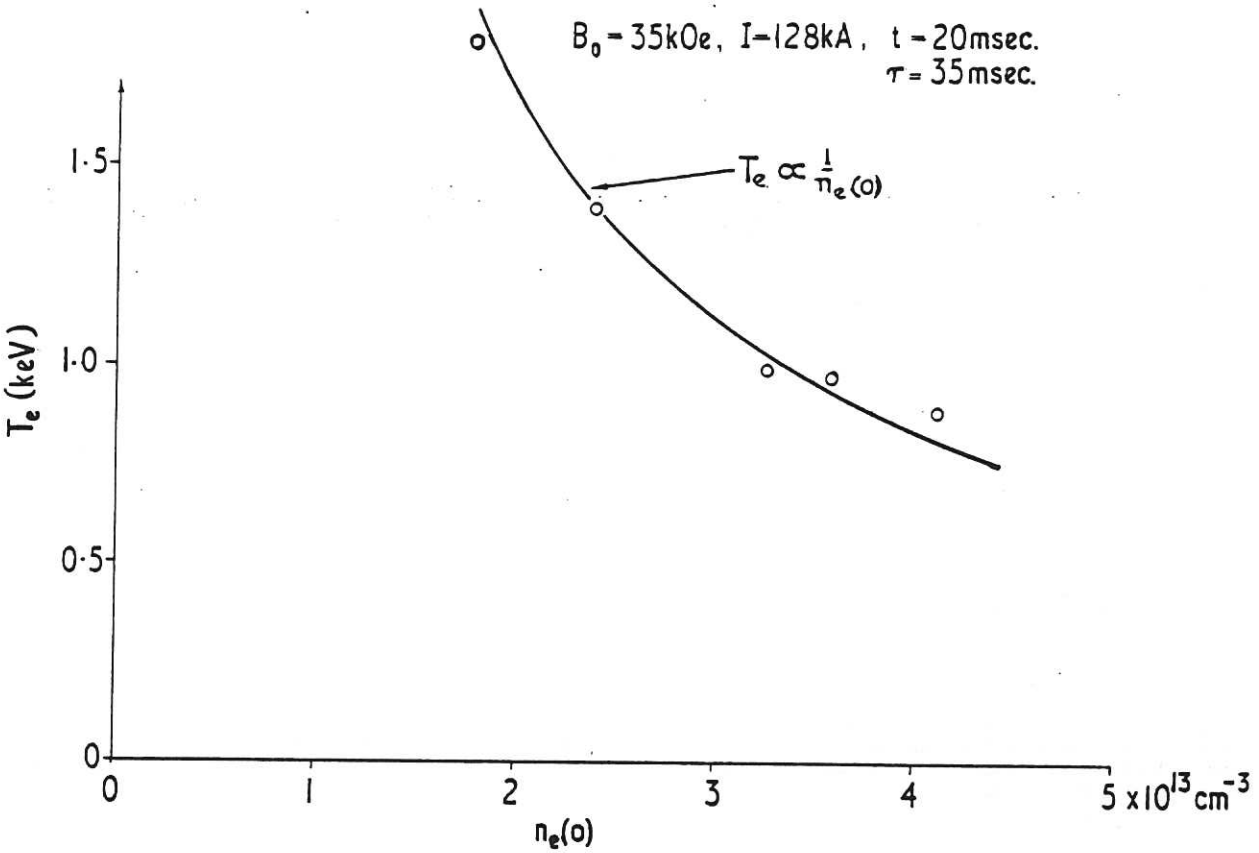

Fig.19 Electron temperature as a function of electron density for a maximum current of 128 kA. The dotted curve shows an inverse dependence on the concentration.

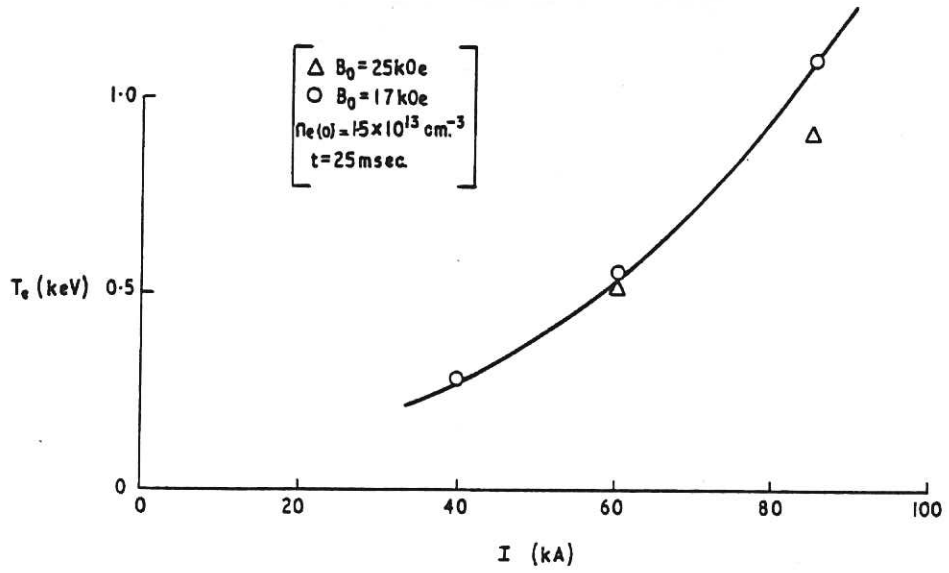

Fig.20 Electron temperature as a function of plasma current for constant electron density, and two values of the stabilising field, 17 and 25 kOe. The full curve shows a quadratic dependance on the current.

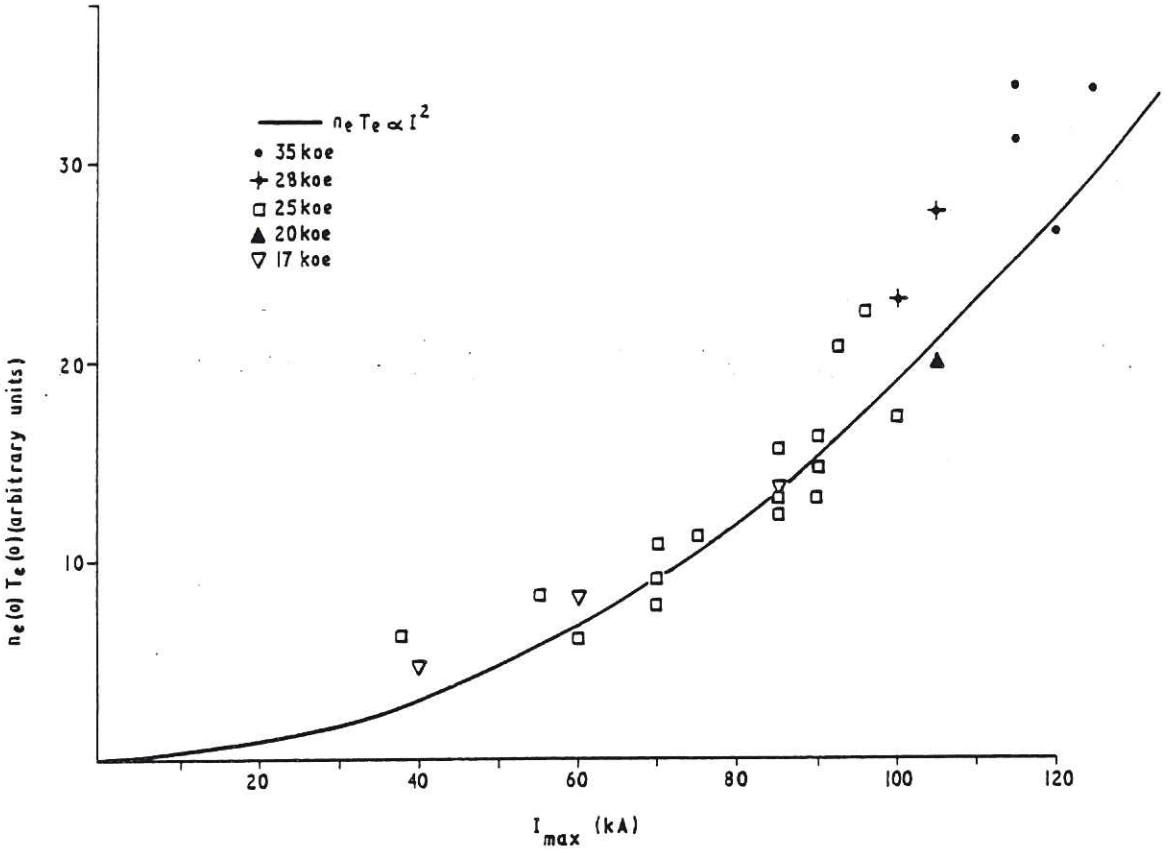

Fig.21 Product of electron density and temperature on axis from Thomson scattering as a function of the plasma current, for stabilising fields from 17 to 35 kOe. The maximum value for the temperature and the density at that time, is used for each discharge. The curve shows a quadratic dependence on the current.

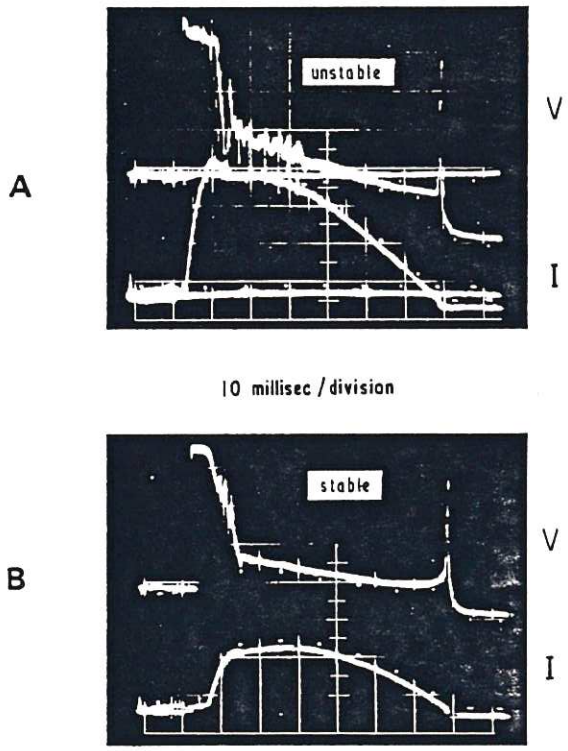

Fig.22 Current and voltage oscillograms for unstable and stable operating conditions.
(a) shows a weakly unstable discharge, where the current waveform is unchanged. Higher currents lead to abrupt changes in the current as well. Note the periodic nature of the 'instability', producing a voltage spike every 3–4 msecs.
(b) shows a stable discharge.

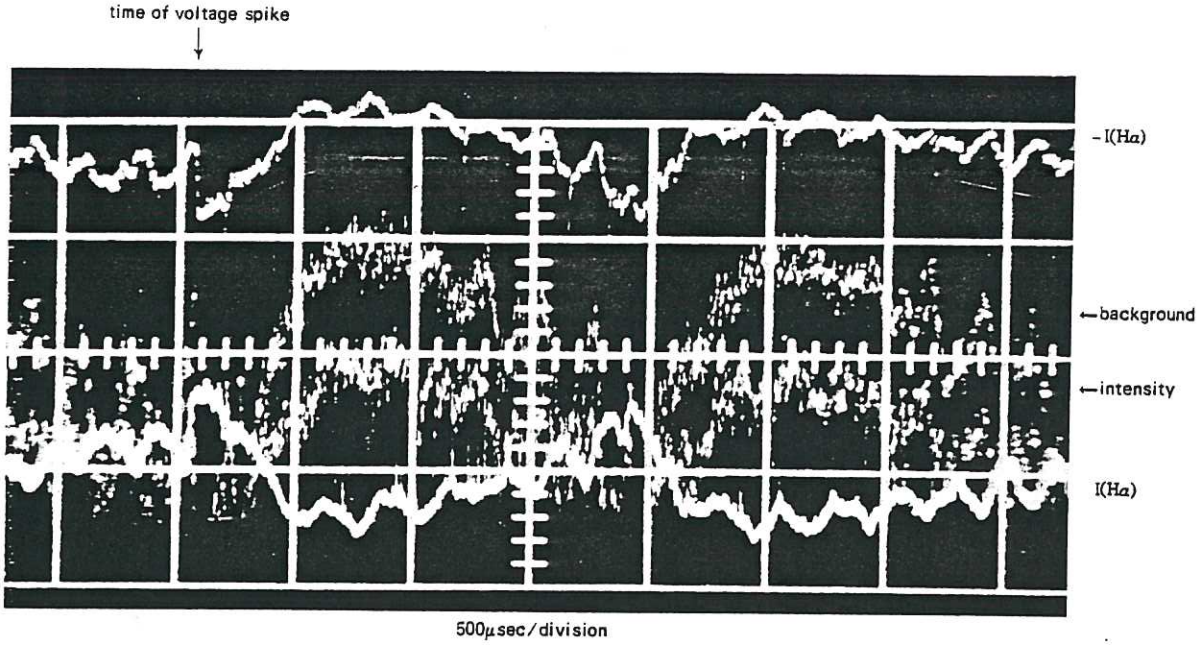

Fig.23 Intensity of Hα, arising from an annular ring around the plasma, under unstable conditions. A voltage spike corresponds to a rapid increase in intensity ($t < 20$ μsecs), probably due to an MHD instability near the outer boundary. Low frequency oscillations are also evident between each voltage spike.

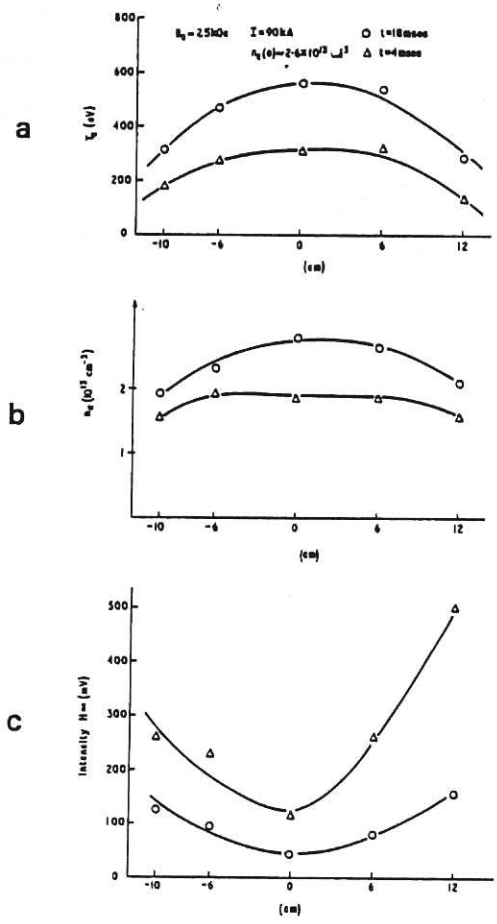

Fig.24 (a) Radial temperature profiles in the vertical plane of a minor cross section for two times, 4 and 18 msec, showing the symmetry about the magnetic axis.
(b) Radial density profiles
(c) Radial intensity profiles of Hα

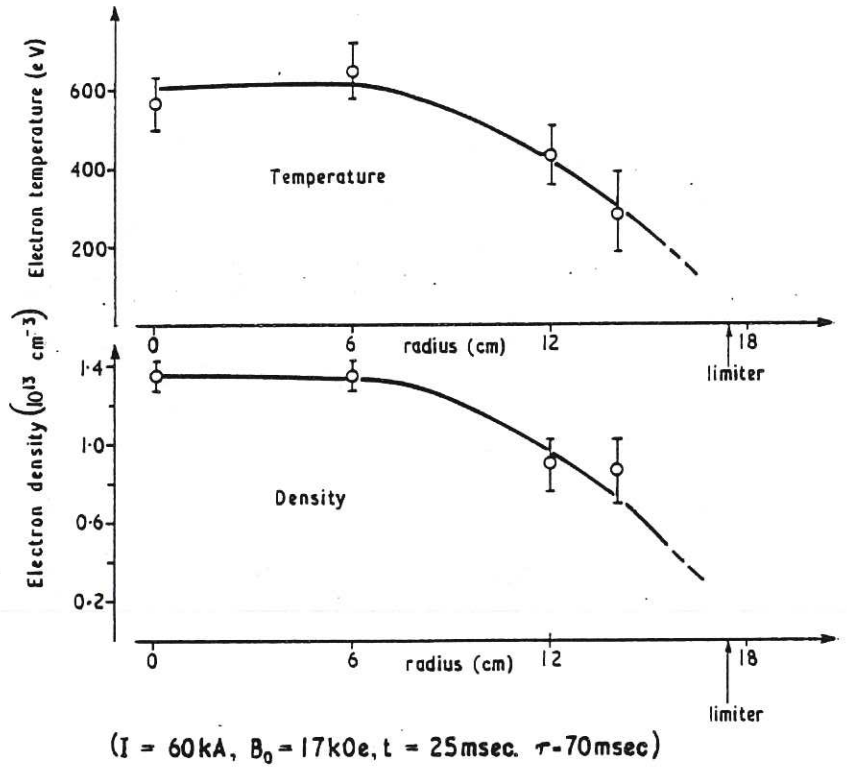

Fig.25 Radial variation of electron temperature and density from Thomson scattering at t = 25 msec for a discharge of 70 msec duration.

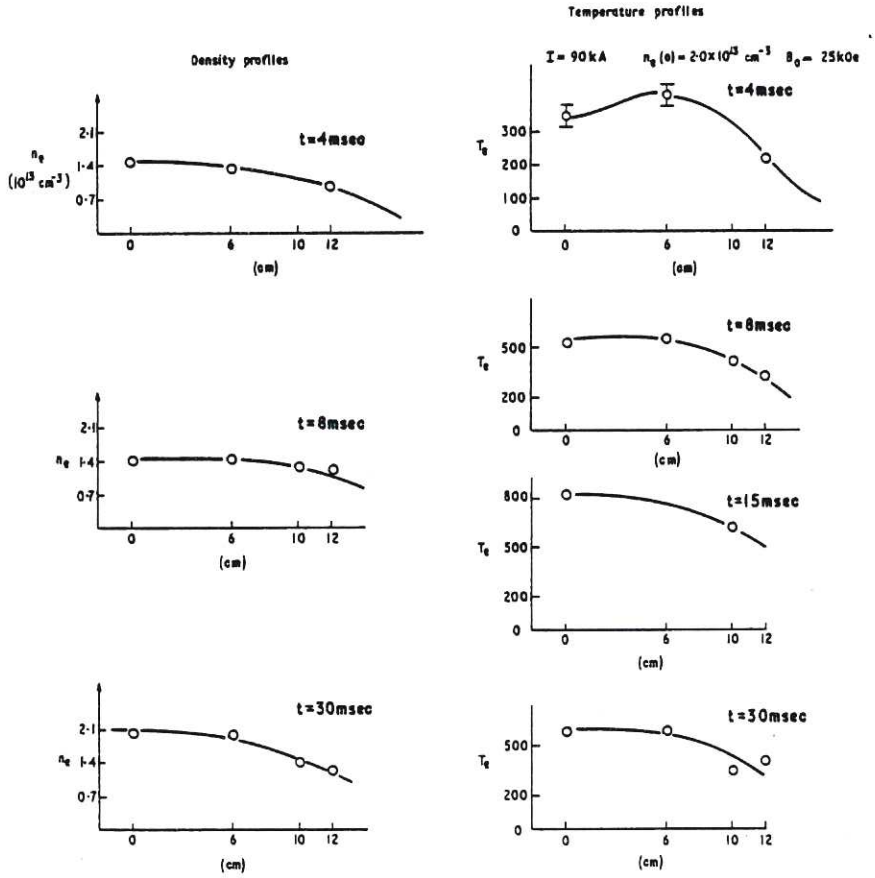

Fig.26 Temperature and density profiles from Thomson scattering for various times throughout a discharge of 35 msecs duration and maximum gas current 90 kA. Note the weak skin effect in the temperature profile at early times. CLM - R 107

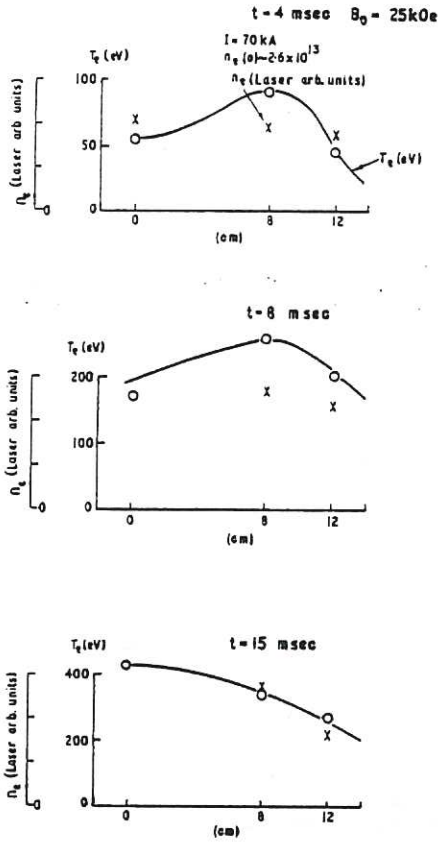

Fig.27 Temperature and density profiles during the heating phase of the discharge showing a weak skin effect (density slightly higher than for Figure 26).

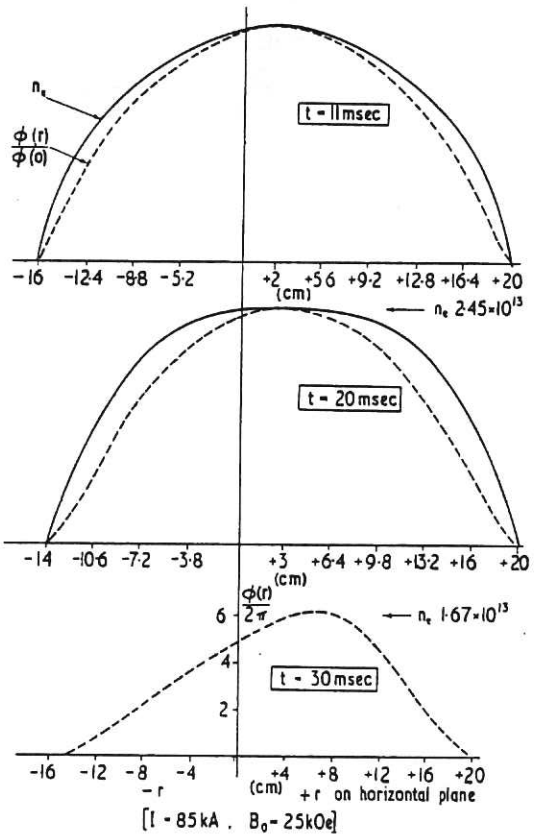

Fig.28 Electron density profiles obtained from the multi-channel microwave interferometer for a case where the plasma experiences a relatively large horizontal displacement. ϕ is the phase shift.

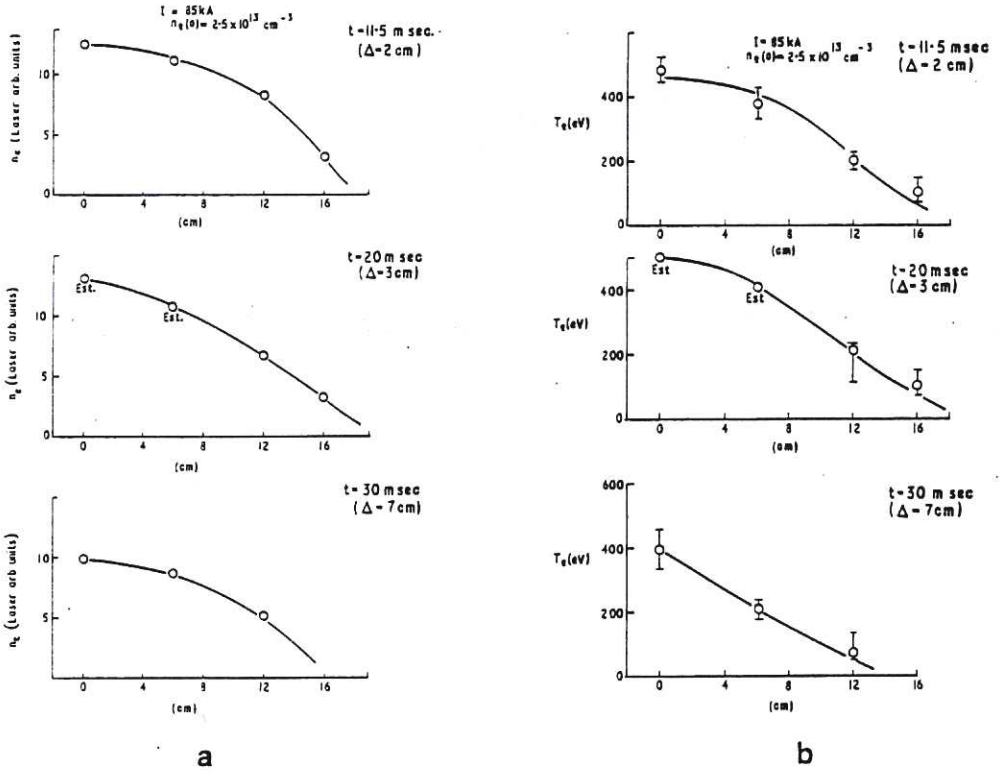

Fig.29 (a) and (b) The temperature and density profiles in the vertical plane obtained by Thomson scattering for the case when the displacement is large (Fig.28). Here Δ denotes the displacement in the horizontal plane. The points marked EST are estimated from the temporal variation at that particular radius.

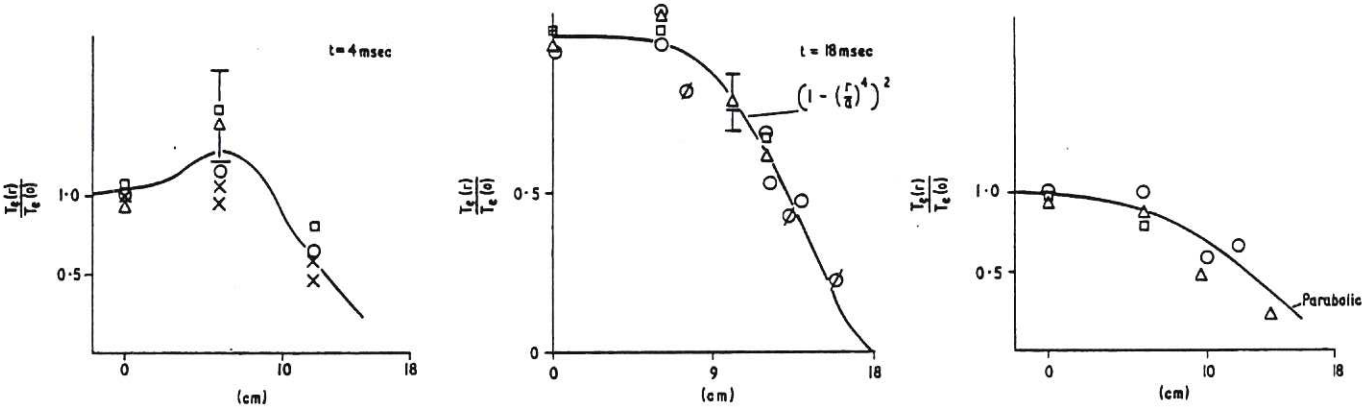

Fig.30 Graphical summary of the radial temperature profiles for times of 4, 18, and 30 msecs, all normalised to unity on axis. A weak skin effect is evident at 4 msecs. The profile shown at 18 msec follows the relation

$$\frac{Te(r)}{Te(o)} = (1 - (r/a)^4)^2 \ ,$$

and at 30 msecs is close to parabolic. The different points refer to data for various conditions from previous diagrams and other results.

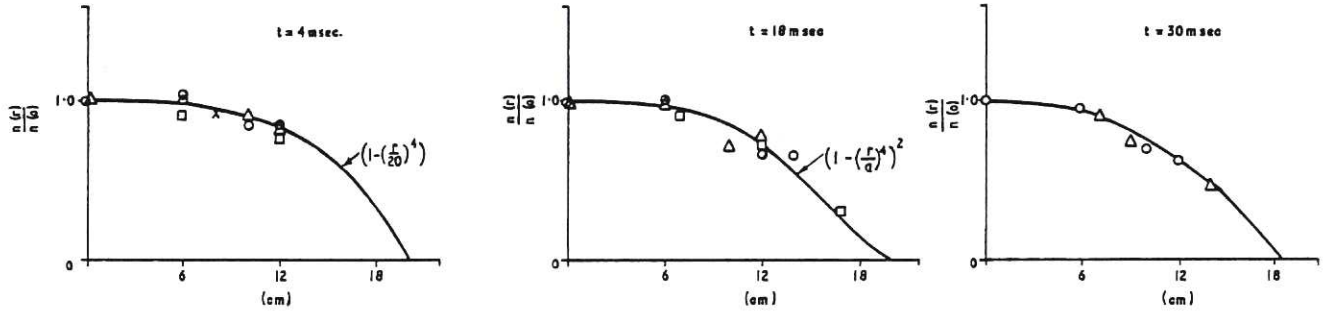

Fig.31 Graphical summary of the radial density profiles for times of 4, 18 and 30 msecs, all normalised to unity on axis. At 4 msecs the profile is approximately given by

$$\frac{n_e(r)}{n_e(o)} = \left(1 - \left(\frac{r}{20}\right)^4\right)$$

and at 18 msec by $(1 - r^4/a^4)^2$. The profiles from the microwave interferometer are similar. CLM – R 107

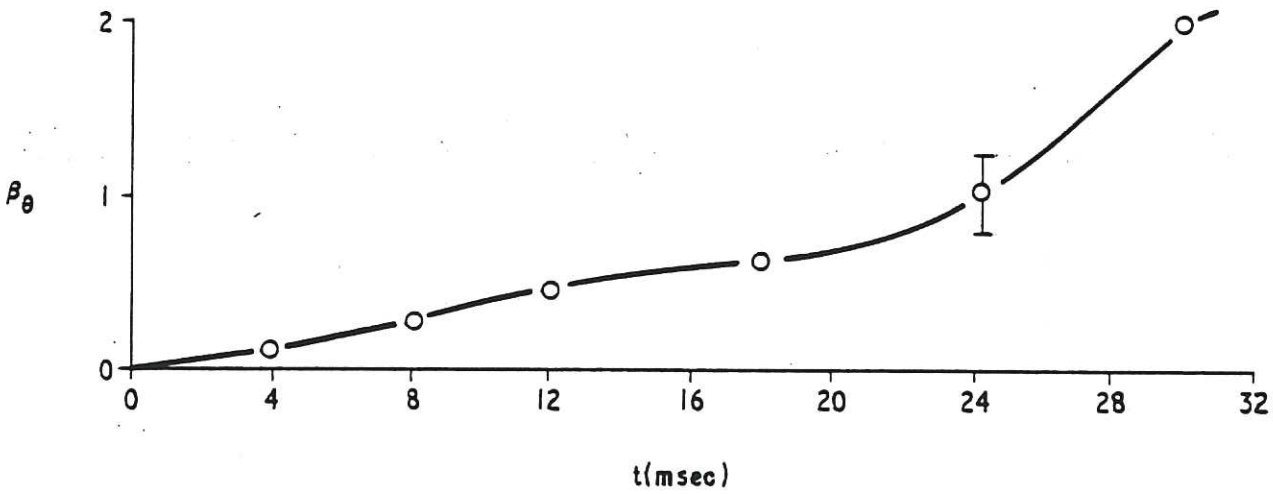

Fig.32 Temporal variation of β_θ for the results shown in Fig.16.

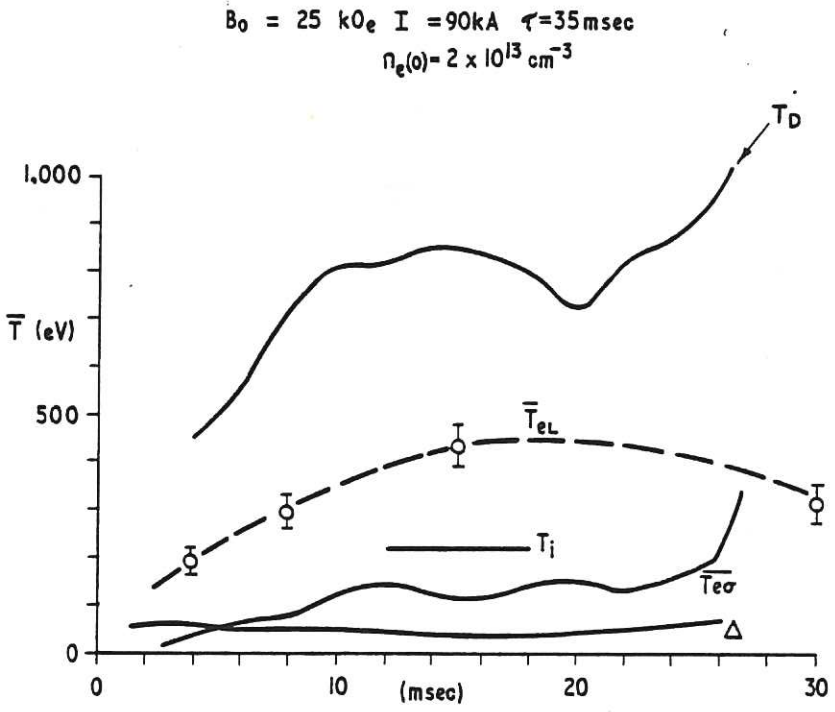

Fig.33 A comparison of the mean temperature deduced from Thomson scattering $\bar{T}_{eL}$, resistance measurements $\bar{T}_{e\sigma}$, and diamagnetic measurements T_D. The ion temperature obtained from the neutral particle analyser is also shown. Δ denotes the horizontal displacement which is constant at about 1 cm.

CLM-R 107

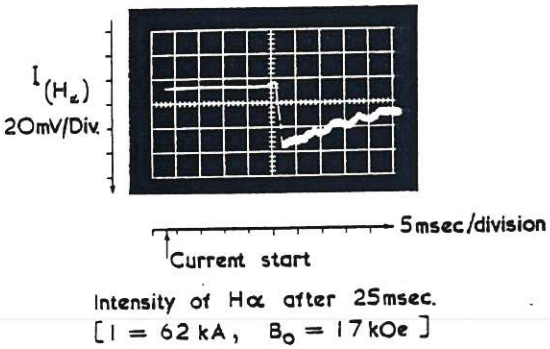

Fig.34 Temporal variation of the intensity of Hα, 25 msecs from the initial current pulse. The rise in signal indicates the opening of the mechanical shutter and the modulation is due to shutter bounce.

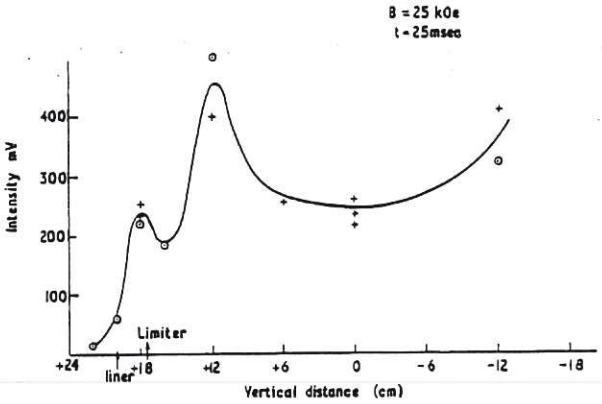

Fig.35 Variation of the intensity of Hα at t = 25 msecs as a function of the vertical distance, for a pulse of 70 msec duration. The different symbols denote separate runs.

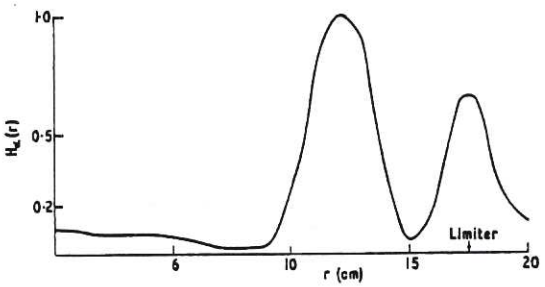

Fig.36 Intensity of Hα as a function of radius after Abel inversion.

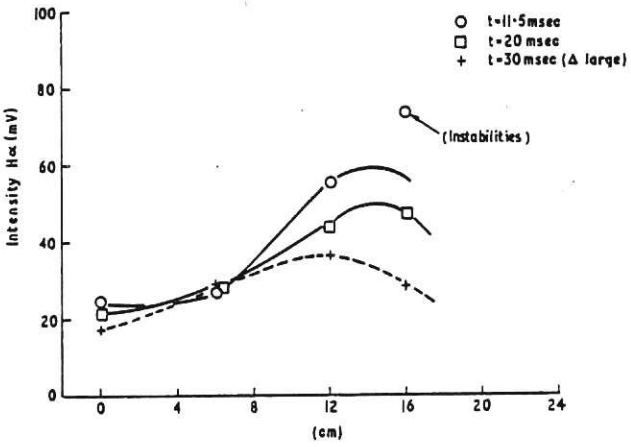

Fig.37 The radial variation of Hα for different times. The point labelled instabilities corresponds to a case where weak instabilities were observed.

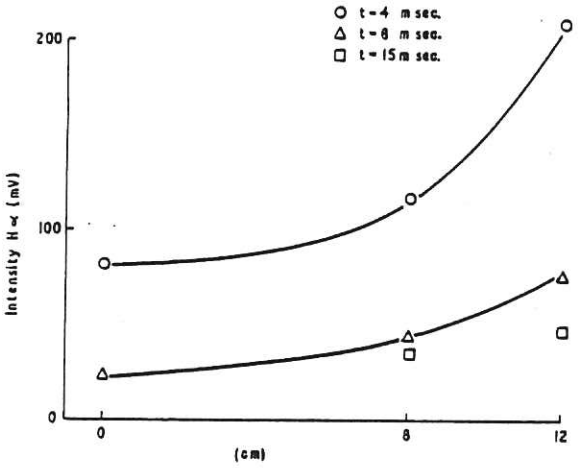

Fig.38 The radial variation of Hα and its decrease in time during the heating phase of the discharge.

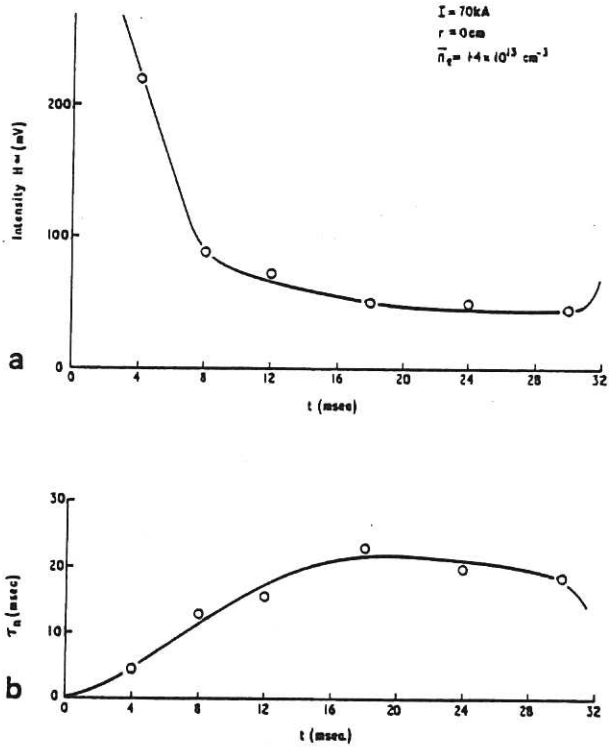

Fig.39 (a) The temporal variation of Hα and (b) the calculated particle confinement time as a function of time. Later than 32 msec there is a rapid increase in Hα associated with the end of the current pulse.

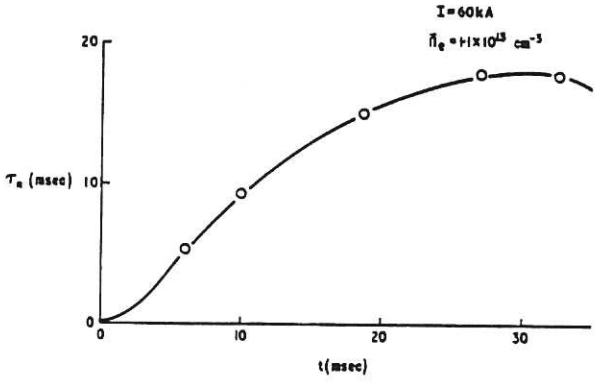

Fig.40 The particle confinement time as a function of time for a plasma current of 60 kA and mean density of 1.1×10^{13} cm^{-3}.

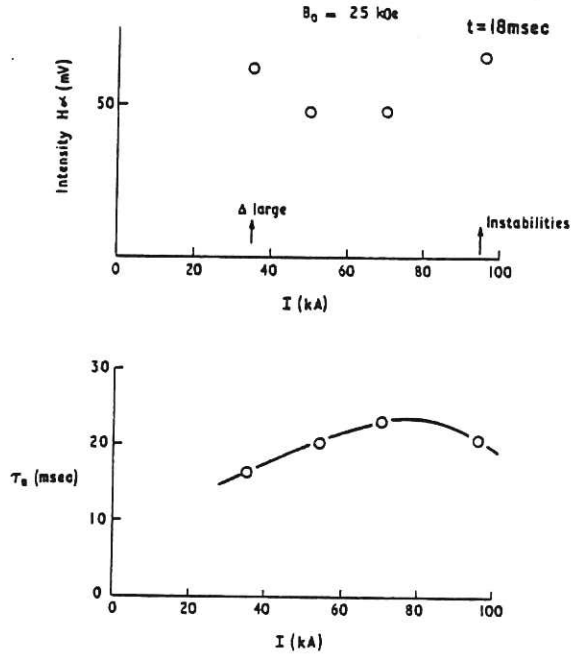

Fig.41 The intensity of Hα and particle confinement time as a function of the current. Weak instabilities were observed at a plasma current of 95 kA for B_0 = 25 kOe, and a large displacement for 35 kA.

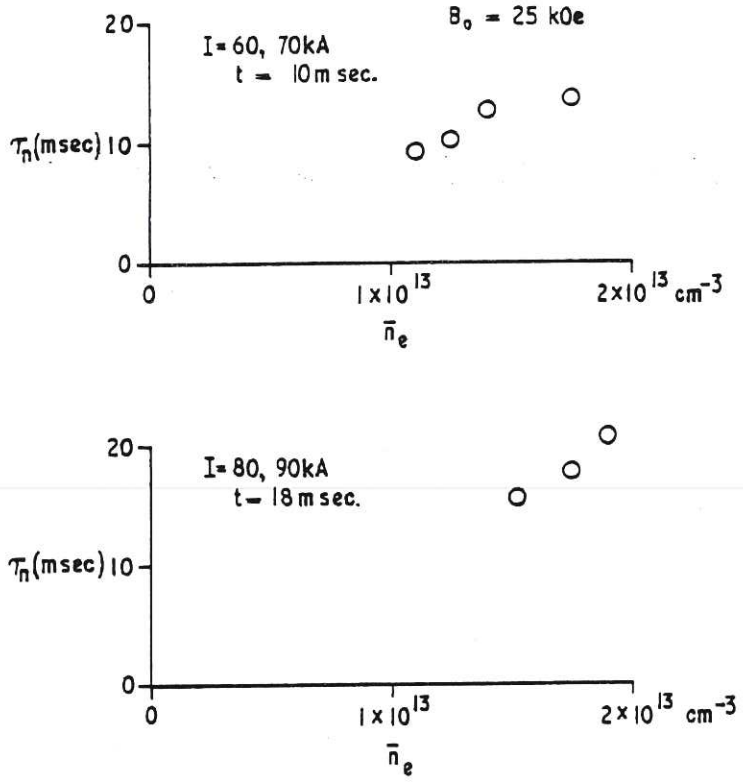

Fig.42 Dependence of the particle confinement time on the average electron density for the range of conditions studied.

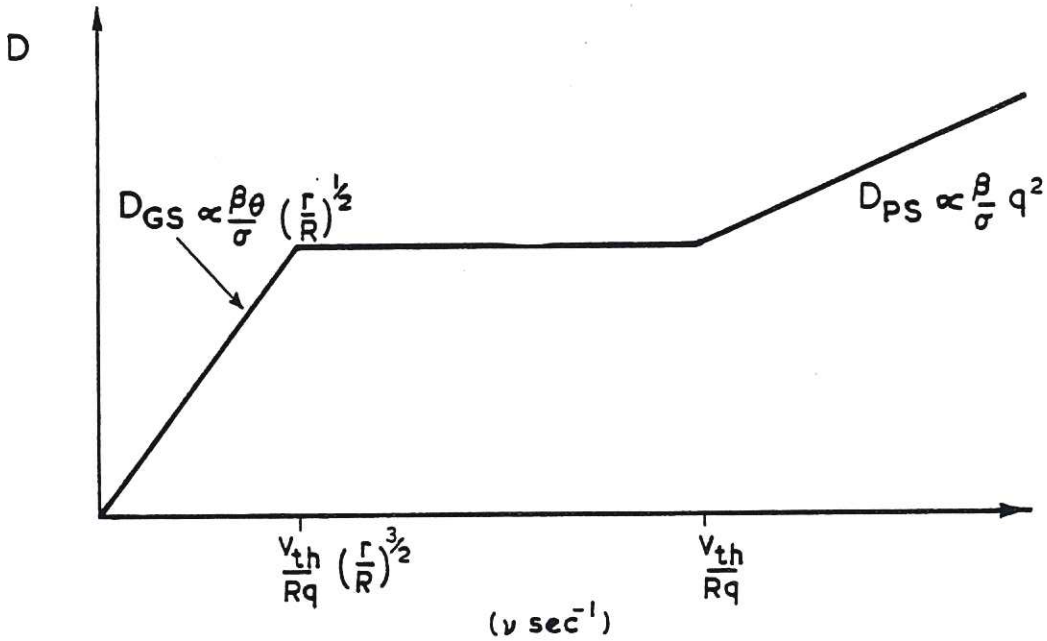

Fig.43 Classical diffusion coefficient as a function of the collision frequency, ν. D_{ps} refers to the Pfirsch-Schluter regime and D_{Gs} to the Galeev-Sagdeev trapped particle regime. v_{th} is the electron thermal speed and the other symbols have their usual meaning.

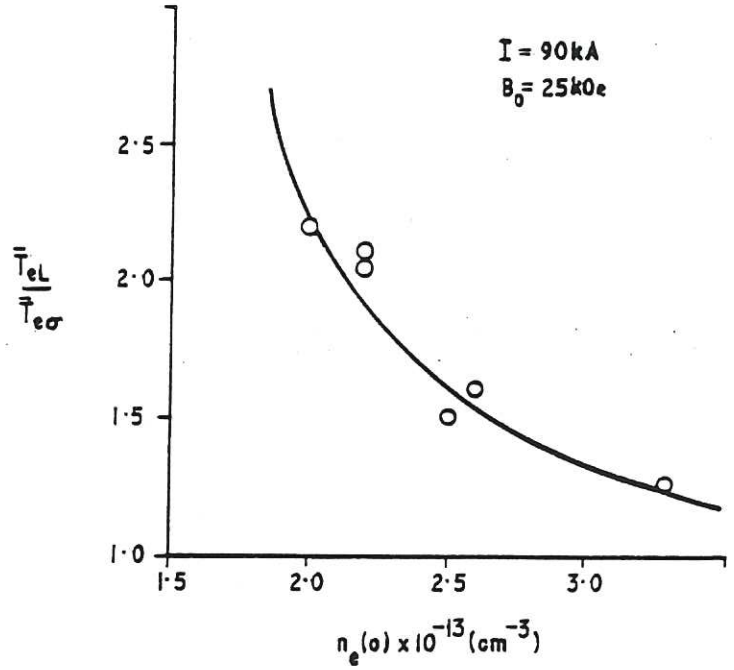

Fig.44 The variation of $\bar{T}_{eL}/\bar{T}_{e\sigma}$ as a function of the electron concentration.

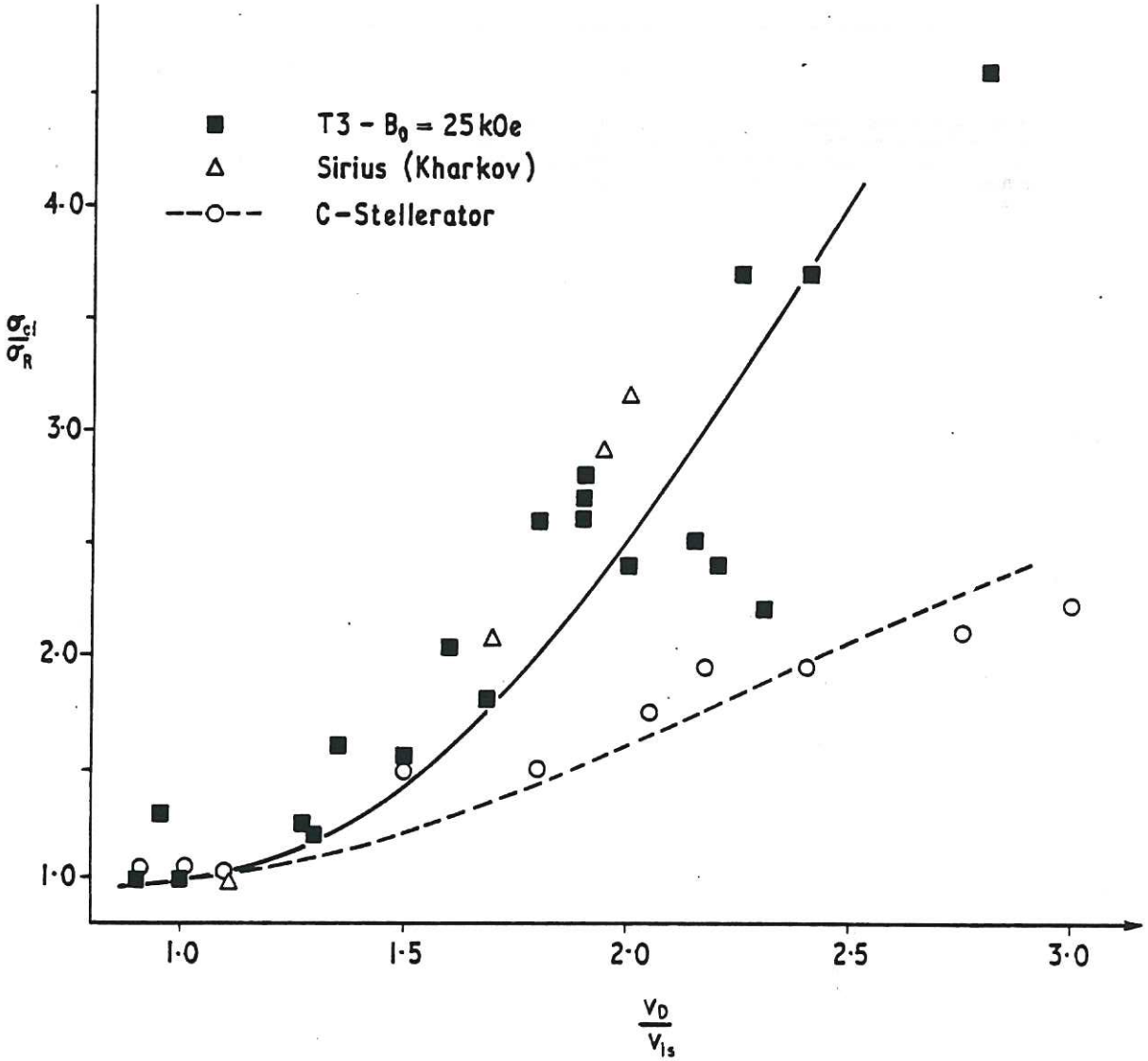

Fig.45 $\sigma_{c\ell}/\sigma_R$ as a function of the ratio of drift to sound speeds V_d/v_{is}, where $\sigma_{c\ell}$ is the Spitzer value for the conductivity. Results from other experimental devices are also indicated.

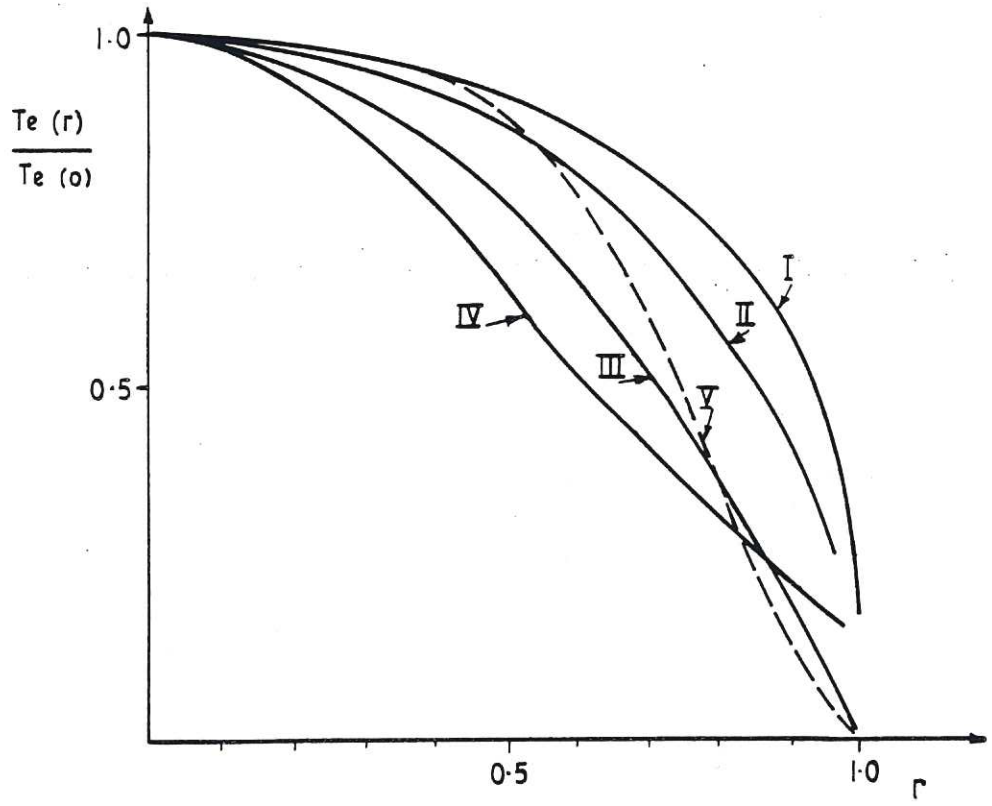

Fig.46 Normalised temperature profiles as a function of the normalised radius, r/a, for losses due to electron thermal conductivity, K_e. I for $K_e \propto T_e^{5/2}$, II $K_e \propto T_e^{3/2}$, III K_e independent of temperature and density, IV losses due to convection [25] and V the experimental profile.

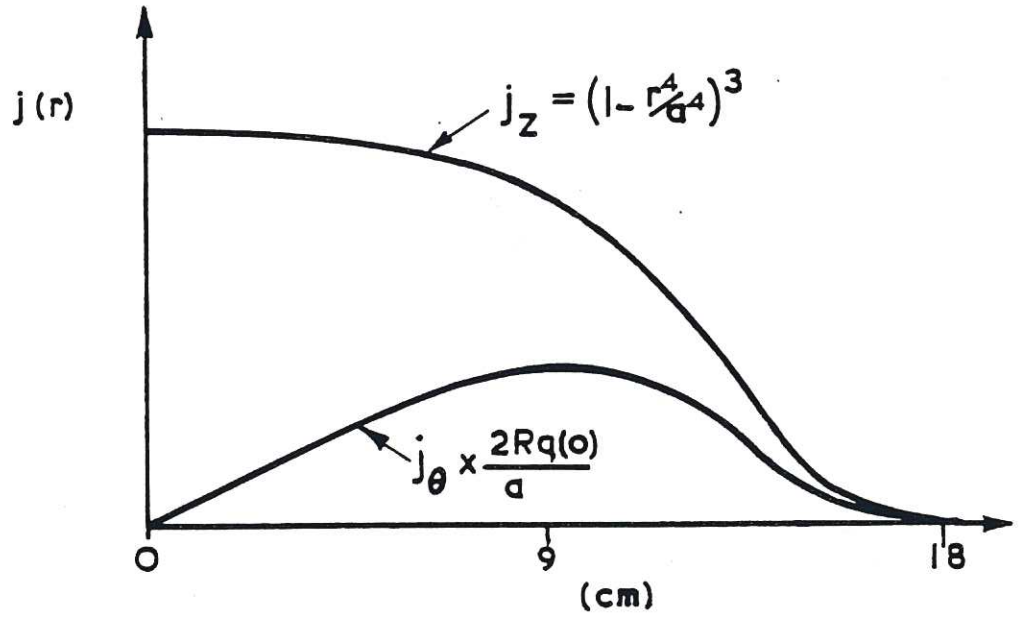

Fig.47 Suggested current density profiles at temperature maximum. Both j_z and j_θ are shown with the latter magnified by more than twenty times.

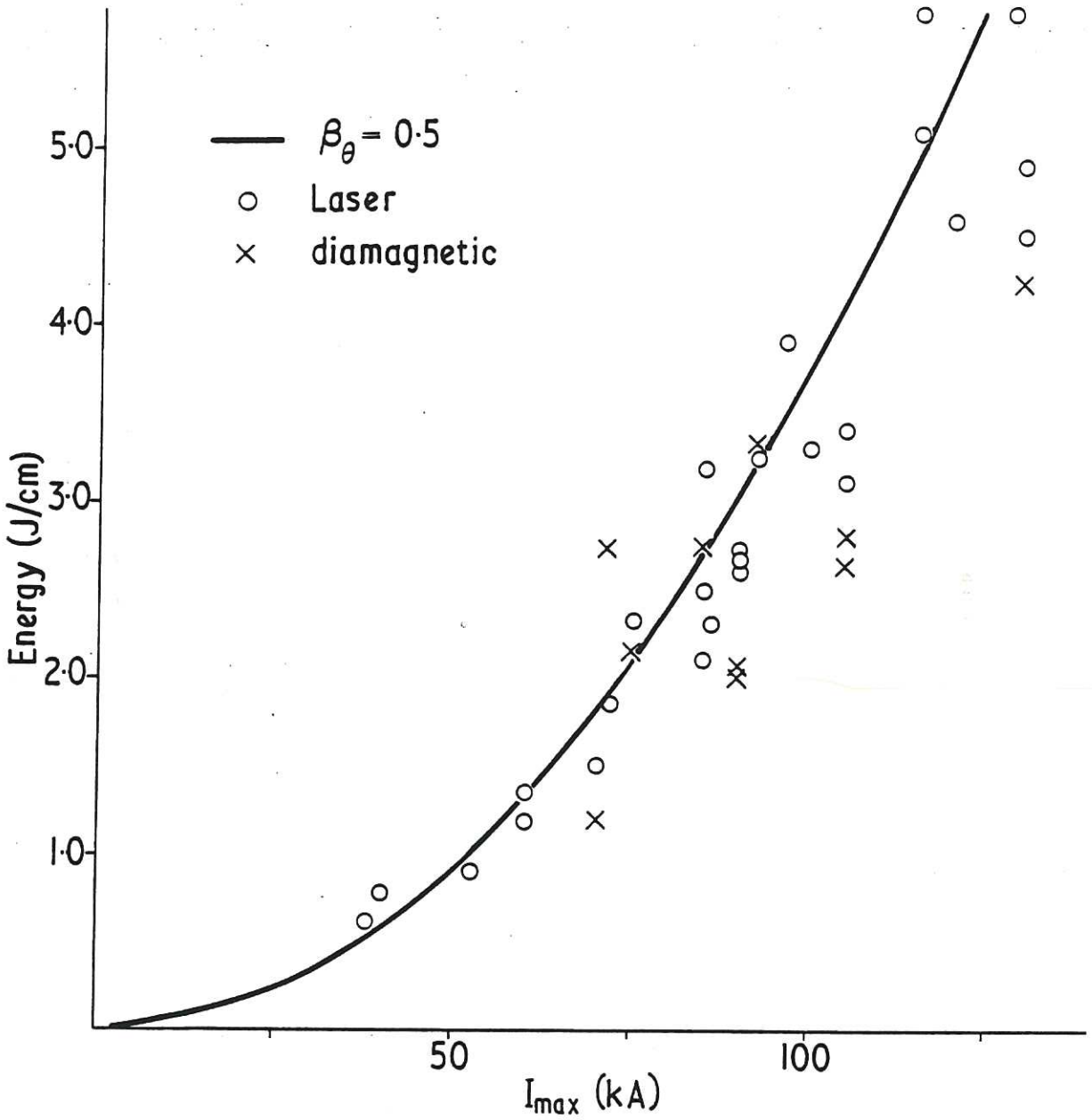

Fig.48 Total plasma energy (joules/cm) as a function of the gas current showing the curve for $\beta_\theta = 0.5$ in the relation $\beta_\theta I^2 = 200\ NkT$. Points obtained by diamagnetic measurements are marked X, and those derived from Thomson scattering and ion temperature measurements by O. CLM-R 107

Available from

HER MAJESTY'S STATIONERY OFFICE

49 High Holborn, London, W.C.1
13a Castle Street, Edinburgh 2
109 St. Mary Street, Cardiff CF1 1JW
Brazennose Street, Manchester M60 8AS
50 Fairfax Street, Bristol BS1 3DE
258 Broad Street, Birmingham 1
7-11 Linenhall Street, Belfast BT2 8AY

or through any bookseller.